Advanced Materials
Research and Technology

https://www.techsyncpress.com

A Review of Propane Dehydrogenation Research Based on Density Functional Theory - Part I

Z. Song

Taizhou University
Taizhou, China
E-mail: songzj@tzc.edu.cn

ABSTRACT: This part covers the industrial background of propane dehydrogenation, the motivation for DFT-based catalyst research, and the main progress on platinum-, chromium-, vanadium-, gallium-, zinc-, boron-, and other catalyst systems.

KEYWORDS: PROPANE DEHYDROGENATION; DENSITY FUNCTIONAL THEORY; CATALYST DESIGN; PLATINUM CATALYSTS; CHROMIUM CATALYSTS; VANADIUM CATALYSTS

1. Introduction

1.1 Industrial Background and Research Significance of Propane Dehydrogenation

Propylene, as a core feedstock in the petrochemical industry, is widely used in the production of high-demand chemicals such as polypropylene, propylene oxide, and acrylonitrile, with market demand continuously rising alongside global industrialization. Traditional propylene production relies primarily on petroleum-based routes such as naphtha steam cracking and catalytic cracking, which suffer from high energy consumption, limited propylene yields, and complex product distributions, making them inadequate to meet current escalating market demands. In recent years, the maturation of shale gas extraction technology has substantially increased propane resource availability and significantly reduced costs, positioning propane dehydrogenation (PDH) technology as a key alternative to traditional routes due to its simplified process, high feedstock utilization, and outstanding propylene selectivity. Currently, mainstream industrial PDH processes employ two main catalyst types: chromium-based catalysts used in the Catofin process and platinum-based catalysts used in catalytic dehydrogenation processes. Among these, platinum-based catalysts are more environmentally favorable, though they suffer from Pt particle sintering and carbon deposition under high-temperature reaction conditions, leading to rapid catalyst deactivation and limiting industrial application efficiency. Chromium-based catalysts face issues of chromium species toxicity and rapid deactivation, inconsistent with green chemistry development trends.

Therefore, developing efficient, stable, and cost-effective PDH catalysts has become the core bottleneck for large-scale application of this technology. Researchers have continuously optimized catalyst

performance through strategies such as alloying, support modification, and dopant incorporation. Notable examples include the development of Pt-In single-atom alloy (SAA) catalysts, which achieved outstanding stability over 60 hours of continuous reaction with only 0.1 w.t.% Pt loading, delivering a propylene formation rate of 23.2 $mol \cdot g^{-1}Pt \cdot h^{-1}$. [1] Through trace boron doping to construct Pt-B cluster structures, Pt sintering was significantly suppressed and Pt species redistribution during reaction was achieved, extending catalyst single-pass lifetime to three times that of traditional Pt-Sn catalysts, as shown in Fig. 1(h). [2] Additionally, Y_2O_3-modified δ-Al_2O_3 supports were employed to regulate PtIn alloy dispersion, further enhancing catalytic stability. [3]

From energy and environmental perspectives, the strongly endothermic nature of the PDH reaction (ΔH_{298}° = 124.3 $kJ \cdot mol^{-1}$) necessitates maintaining industrial temperatures of 570-650 °C, resulting not only in enormous energy consumption but also accelerating catalyst deactivation. The oxidative dehydrogenation route using CO_2 as a soft oxidant (CO_2-ODHP) can utilize CO_2 to consume the H_2 generated by the reaction, thereby breaking thermodynamic equilibrium limitations and enhancing propylene yields, while simultaneously achieving CO_2 resource utilization, aligning with low-carbon chemical industry development needs under "dual carbon" goals. Related research includes the design of Pt-Sn/ZrO_2-CaO bifunctional materials that achieve integrated CO_2 capture and conversion at 600°C with propylene selectivity exceeding 98 %. Photothermal synergistic mechanisms have been employed to enhance coupling between CO_2 activation and propane dehydrogenation, providing new approaches for low-temperature, high-efficiency CO_2-ODHP. [4] Machine learning combined with density functional theorem (DFT) calculations has been leveraged to optimize Cr-Ni-Co-ZrO_x multicomponent catalysts, significantly improving propylene yields and CO_2 conversion rates.[5] However, CO_2-ODHP still faces challenges including difficult CO_2 activation and excessive propane cracking, urgently requiring breakthroughs through catalyst structural design and reaction mechanism optimization.

In the non-precious metal catalyst domain, zinc-based catalysts have emerged as potential alternatives to Pt-based and Cr-based catalysts due to their low cost and low toxicity. Traditional ZnO/Al_2O_3 catalysts readily form inert $ZnAl_2O_4$ spinel phases at high temperatures, but hydroxyl-deficient Al_2O_3 supports can effectively suppress this phase transformation, maintaining ZnO in highly active nanocluster form and significantly enhancing catalytic stability. [6] Co-Zr co-doped CeO_2 nanorods have been constructed with oxygen vacancy-rich structures, leveraging photothermal synergistic effects to reduce reaction temperatures, achieving propane conversion and propylene selectivity of 230.04 $\mu mol \cdot g^{-1}cat$ and 90.3 %, respectively. [7]

At the fundamental research level, the rapid development of computational chemistry methods such as density functional theory (DFT) has provided atomic-level perspectives for PDH research [Fig. 1(e)]. Through DFT calculations, researchers can precisely analyze catalyst active site structures, reaction intermediate evolution pathways, and reactant/product adsorption-desorption behaviors, providing theoretical guidance for catalyst design. For instance, DFT can elucidate the regulatory mechanism of In on Pt electronic structure and geometric configuration in Pt-In SAA,[1] reveal the enhancement effect of oxygen vacancies on photothermal catalytic performance in Co-Zr co-doped CeO_2 nanorods (Fig. 1), [7] or clarify the influence of hydroxyl content on $ZnAl_2O_4$ spinel phase formation in ZnO/Al_2O_3 systems, providing core support for rational design of high-performance catalysts.[6] DFT combined with microkinetic simulations has revealed the structure sensitivity of different Pt facets, (111), (100), (110), (211) and the regulatory mechanism of hydrogen coverage effects on reaction pathways, providing theoretical basis for Pt-based catalyst size optimization.[8]

Furthermore, industrial advancement of PDH technology requires bridging theory and experiment. Current research has progressively clarified catalyst structure-performance relationships, reaction mechanisms, and deactivation mechanisms through integration of DFT with microkinetic simulations and in situ characterization techniques (such as in situ DRIFTS and AC-HAADF-STEM), providing critical foundations for catalyst performance optimization and industrial condition adaptation. Developing novel catalysts with low Pt loading and high stability (such as single-atom alloys and bifunctional catalysts), elucidating the mechanism of soft oxidants like CO_2, and achieving precise control of multiscale reaction processes have become research hotspots and core objectives in the PDH field. Therefore, conducting fundamental research and application development of PDH technology not only holds significant industrial

application value but can also provide theoretical and technical support for low-carbon chemical technology innovation.

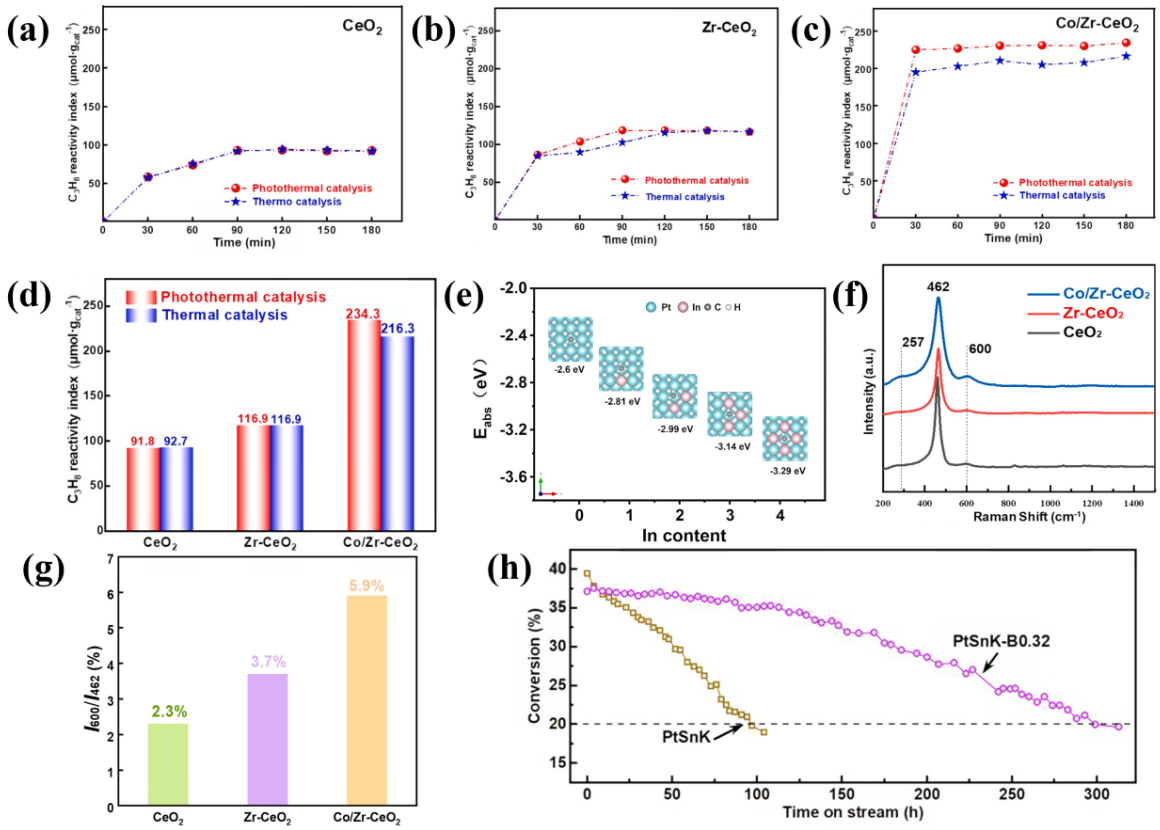

Figure 1. Comparison of propane dehydrogenation performance under purely thermal and photothermal conditions at 300 ◦C for (a) CeO2, (b) Zr-CeO2, and (c) Co/ZrCeO2, respectively. (d) The representative values at the testing time of 180 min. (e) DFT-calculated CH_3 adsorption energies on a Pt site with varying numbers of In atoms. (f) Raman spectra of CeO2, Zr-CeO2, and Co/Zr-CeO2 nanorods; (g) Defectiveness comparison calculating from intensity ratios of I600/I462, respectively. (h) Propane conversion

1.2 Overview of Density Functional Theory Applications in Catalysis Research

Density functional theory (DFT), as a core method in computational chemistry, has become an indispensable tool for propane dehydrogenation (PDH) catalysis research due to its precise description capabilities for atomic-scale electronic structures and energy changes, providing atomic-level theoretical support for catalyst design, reaction mechanism analysis, and performance optimization. Its core value lies in efficiently calculating catalyst surface active site configurations, adsorption energies of reactants/intermediates/products, reaction pathway energy barriers, and electronic structure evolution, thereby quantitatively revealing the intrinsic correlation between catalytic performance and microstructure, substantially reducing experimental trial-and-error costs.

In catalyst active site design and optimization, DFT can precisely predict the active center characteristics of systems such as single-atom alloys (SAA), bimetallic alloys, and non-metal-doped structures. For example, DFT calculations revealed that in Pt/Cu single-atom alloys [Fig. 2(c)], Cu modulation of Pt electronic structure and geometric configuration significantly reduces propylene deep dehydrogenation energy barriers and suppresses carbon formation, with C-C bond breaking barriers (>2.0 eV) dramatically exceeding C-H bond activation barriers, providing critical basis for high-selectivity catalyst design.[9] Research on Pd and Cu single atoms supported on β-Mo_2C (001) surfaces demonstrated that DFT clarified metal atoms preferentially anchor at Mo hollow sites [Fig. 2(e)], modulating active center electron density through charge transfer [Fig. 2(a)-(b)], reducing the rate-determining step barrier for propane

dehydrogenation in the Cu_1/Mo_2C system to 0.31 kcal/mol, significantly outperforming pure Mo_2C supports.[10] DFT calculations confirmed that in Ru_1Cu single-atom alloys, the Ru single-atom d-band center approaches the Fermi level, enhancing propane adsorption and C-H bond activation capability, with PDH activity and anti-coking performance surpassing traditional Pt catalysts.[11] Additionally, DFT studies of alloying effects between Pt, Ni-based alloys and post-transition metals such as Sn, Ga, and Bi found that Ni_3Ga alloys superior in both activity and selectivity compared to pure Ni, while Bi alloys exhibited the highest propylene selectivity.[12]

Furthermore, through DFT combined with experimental characterization, NH_3 pyrolysis-induced Ir formation of $Ir\text{-}O_2N_2$ active motifs was revealed [Fig. 3(d)], with unique dual-coordination environments enabling ppm-level loaded Ir_1/NOC catalysts to exhibit excellent PDH performance [Fig. 2(f)].[13] DFT also provides theoretical guidance for doping modifications of non-precious metal catalysts such as boron-based and vanadium-based systems, such as optimizing Mg doping amounts to regulate $VOx@ZrO_2$ surface basicity and oxygen vacancy concentrations, or designing $B\text{-}O_3$ active sites through C-O substitution strategies, achieving precise catalytic performance control.

In reaction mechanism and pathway analysis, DFT can systematically clarify complex pathways in PDH reactions, identifying rate-determining steps (RDS) and selectivity control factors. DFT calculations for Pt-based catalysts revealed that PDH reactions follow a two-step dehydrogenation pathway of "propane→propyl intermediate→propylene," with the first C-H bond activation (barrier 0.78-1.16 eV) as the rate-limiting step [Fig. 3(a)-(b)]. They also clarified that low-coordination atoms on Pt (211) facets have lower C-H activation barriers compared to Pt (111) and Pt (100) facets, making them the core active facets of Pt-based catalysts.[14] In Ni-based alloy systems, DFT identified that Ni_3Ga alloys optimize C_3H_6 and H formation energies (activity descriptors), enhancing dehydrogenation activity while suppressing side reactions such as hydrogenolysis and coking [Fig. 3(e)], with propylene selectivity significantly superior to pure Ni catalysts.[12] For oxidative dehydrogenation (ODH) systems, DFT combined with deep potential molecular dynamics simulations revealed competitive relationships between propane C-C bond breaking and C-H bond activation [Fig. 2(d)], as well as the acceleration effect of ·OH radicals generated from H_2O_2 decomposition on dehydrogenation reactions, providing mechanistic support for regulating reaction selectivity. Additionally, DFT can analyze coupling mechanisms between reverse water-gas shift (RWGS) and dehydrogenation reactions in CO_2-assisted PDH systems, clarifying synergistic effects of CO_2 on lattice oxygen regeneration and coke removal.[15]

In multiscale simulation and theory-experiment integration, DFT calculation results provide core data support for microkinetic simulations and machine learning (ML) model training, achieving cross-scale correlations from atomic scale to macroscopic reaction performance. For example, a bootstrap aggregating regression (BAR) model trained on 92 sets of DFT-calculated C-H bond breaking barrier data can rapidly predict PDH activity of 53 single-atom alloys, successfully screening high-performance catalysts such as Ru_1Cu.[11] Combining DFT with kinetic Monte Carlo (kMC) simulations enables quantification of surface species coverage evolution and catalyst deactivation patterns [Fig. 3(c)], such as formation pathways and suppression mechanisms of coking precursors like $CH_3CH_2C^*$ in Pt/Cu single-atom alloys.[9] The development and validation of ReaxFF reactive force fields, benchmarked against DFT-calculated intermediate energies and bond-breaking barriers, achieves efficient simulation of PDH reaction dynamic processes in large-scale systems, with the developed 2023-Pt/C/H force field accurately reproducing reactive activity order of different Pt facets.[14] Meanwhile, integration of DFT with in situ characterization techniques (such as in situ XAFS and DRIFTS) enables theoretical validation of experimentally observed active site valence changes and intermediate structures, forming a closed-loop research paradigm of "experimental characterization - theoretical verification - performance optimization".

In summary, DFT has played a core role in active site design, reaction mechanism analysis, deactivation mechanism exploration, and multiscale simulation integration for PDH catalysts, with applications spanning the entire process from rational catalyst design to industrial condition adaptation. With improvements in functional accuracy (such as DFT+U, DFT-D4), integration of dynamic simulation methods (such as AIMD) with machine learning, DFT is poised to further overcome bottlenecks in complex system descriptions and long-timescale kinetic simulations, providing more powerful theoretical support for PDH technology development toward high efficiency, stability, and low-carbon directions.

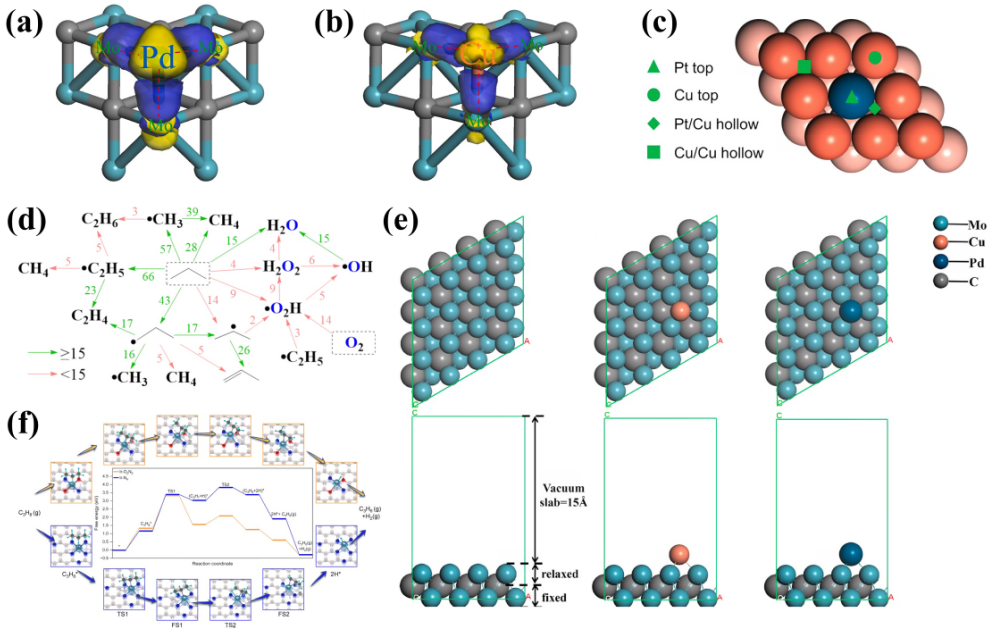

Figure 2. Differential charge density of (a) Pd1/Mo2C and (b) Cu1/Mo2C. (blue represents regions of charge accumulation, yellow represents regions of charge depletion). (c) Top view of the Pt/Cu SAA (111) catalytic surface and the sites designed in the simulation as distinguished by different green shapes. (d) Evolution network of species. The numbers next to the arrows represent the turnover number of the elementary steps, and the colors serve to distinguish reactions according to their presence, using a threshold of 15 occurrences. (e) Top view and side view of $Mo_2C(001)$ surface. Top view and side view of $Cu/Mo_2C(001)$ surface. Top view and side view of $Pd/Mo_2C(001)$ surrface. (f) ofiles of PDH on $Ir{-}O_2N_2$ and $Ir{-}N_4$ configurations at 600 °C. The partial pressures of C_3H_8 and H_2 were set to 0.1 atm, while that of C_3H_6 was set to 0.03 atm. TS: transition state; FS: final state. Color scheme: H, lake blue; C in adsorbate, dark gray; C in support, gray; N, blue; O, red; Ir, light cyan.

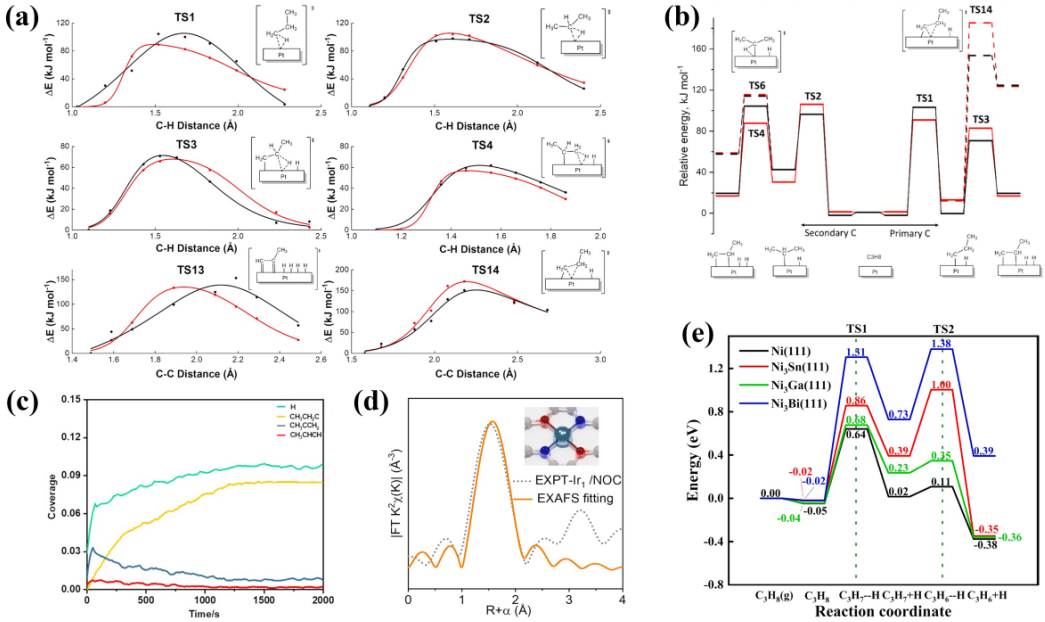

Figure 3. (a) Comparison of ReaxFF and DFT energy scans of four C−H bond activations and two C−C bond activations. Black and red lines correspond to ReaxFF and DFT calculations, respectively. Energies

are in kJ mol−1 and distances in Å. (b) Comparison of ReaxFF and DFT energy profile (kJ mol−1) for propane dehydrogenation reaction on Pt(111) surface starting by a C−H activation at primary carbon and at secondary carbon. Black and red lines correspond to ReaxFF and DFT calculations, respectively, while dashed lines correspond to side reactions. (c) all surface species on a time scale of 2000 s. (d) The EXAFS spectra curve-fitting of the Ir−O_2N_2 model (e) The potential energy diagram of PDH for Ni-based catalysts.

2. DFT Research Progress on Different Catalyst Systems

2.1 Platinum-Based Catalysts

Platinum (Pt)-based catalysts have become core research systems for propane dehydrogenation (PDH) reactions due to their excellent C-H bond activation capabilities, with catalytic performance and reaction mechanisms of monometallic, alloyed, and single-atom alloy forms deeply analyzed through density functional theory (DFT) calculations. DFT calculations not only reveal structure-performance relationships of Pt-based catalysts but also provide critical theoretical support for alloy element screening and active site optimization.

2.1.1 Monometallic Pt Catalysts

The PDH performance of monometallic Pt catalysts is closely related to surface facet structures and active site types. DFT studies demonstrate that reaction mechanisms of Pt catalysts exhibit facet dependence: terrace sites such as Pt (111) follow the traditional reverse Horiuti-Polanyi mechanism, generating propylene through two consecutive dehydrogenation steps, where propane first dehydrogenates to form propyl intermediates (1-propyl or 2-propyl), then further dehydrogenates to produce propylene. The energy barrier difference between 1-propyl and 2-propyl pathways is small, with reaction selectivity determined by competition between propylene desorption and deep dehydrogenation.[16] In contrast, low-coordination step sites such as Pt (211) predominantly follow non-reverse Horiuti-Polanyi mechanisms, generating CH_3CCH_2 intermediates through three-step dehydrogenation (removing two β-H and one α-H), then forming propylene via hydrogenation reactions. This pathway contributes over 50% of propylene production and is sensitive to H_2 partial pressure, with optimal H_2/C_3H_8 ratio around 1.33.[16]

Additionally, size effects of monometallic Pt catalysts have been systematically investigated through DFT calculations. Among small Pt clusters (Pt_2-Pt_6), Pt_5 exhibits optimal PDH activity, selectivity, and stability, with low-coordination metal atoms enhancing C-H bond activation capability. Support introduction (γ-Al_2O_3 and g-C_3N_4) significantly modulates catalytic selectivity, with Pt_5/g-C_3N_4 systems showing the most outstanding performance.[17] Through Bayesian statistics combined with DFT calculations, Pt (211) was confirmed as the most relevant active site in Pt catalysts, while evidence for Pt (100) as the dominant active facet was insufficient.[18] Most simulations show that the kinetic rate-controlling step for propane dehydrogenation is the first dehydrogenation of propane to C_3H_7*. More in-depth size effect studies through DFT calculations combined with experimental validation clarified the regulatory role of Pt cluster sizes in the 3-9 nm range on reaction mechanisms: small Pt clusters (predominantly Pt (211) facets) have lower dehydrogenation barriers and higher activity but lower propylene selectivity. Large Pt clusters (predominantly Pt (111) facets) weaken propylene adsorption strength and increase deep dehydrogenation barriers, thereby improving selectivity.[19]

The main challenges for monometallic Pt catalysts lie in carbon formation from deep dehydrogenation and selectivity decline. DFT calculations show that strong propylene adsorption on Pt surfaces readily triggers further dehydrogenation to generate coking precursors such as propyne, while high activity of step sites accelerates side reactions such as C-C bond cleavage.[20] Additionally, Pt particle sintering under high-temperature reaction conditions leads to active site loss, a phenomenon quantitatively explained through DFT-calculated Pt interatomic binding energies and surface diffusion barriers.[2]

2.1.2 PtSn Alloy Catalysts

Tin (Sn) is one of the most commonly used alloying elements for Pt-based catalysts, with its introduction synergistically enhancing PDH performance through geometric and electronic effects, mechanisms confirmed by extensive DFT studies. Through acid etching-reduction experiments combined with DFT calculations, the recoverability of Pt-Sn alloy surfaces was revealed: after acid etching removes surface Sn, core Sn atoms can migrate to the surface to reconstruct Pt_3Sn alloy phases. Even after 5 acid etching-

reduction cycles, propylene selectivity remains at 92%, a phenomenon driven by Sn segregation behavior due to lower surface energy. [21] Geometrically, Sn atom introduction disrupts continuous Pt-Pt active sites, reducing Pt atom agglomeration and decreasing C-C bond cleavage probability. Electronically, electronegativity differences cause electron transfer from Sn to Pt, downshifting Pt d-band centers, weakening adsorption strength of intermediates like propylene, promoting product desorption, and suppressing deep dehydrogenation. [22]

DFT calculations systematically investigated effects of Sn content and alloy structure on catalytic performance. For alloys with different ratios such as Pt_3Sn, Pt_2Sn, and $PtSn_2$, $Pt_3Sn(111)$ was confirmed as the optimal structure balancing activity and selectivity: its propylene desorption barrier decreases by 0.2-0.3 eV while deep dehydrogenation barriers increase by 0.15-0.25 eV [Fig. 4(g)], elevating propylene selectivity from below 70% for monometallic Pt to above 95 %.[22] Focusing on g-C_3N_4-supported Pt_3Sn single-cluster catalysts, Sn introduction promoted propylene desorption and suppressed deep dehydrogenation and carbon formation, with catalytic performance superior to Pt_1 and Pt_4 single-cluster catalysts.[23] Pt_3Sn_1 clusters on γ-Al_2O_3(110) supports exhibited good activity and stability, with Sn addition suppressing Pt sintering through strong Pt-Sn interactions, and optimal catalytic performance at Pt/Sn ratio of 3:1, while 1:1 ratio caused catalyst deactivation.[24]

Comparison of DFT results for surface alloys (such as Pt_3Sn/Pt (111)) versus bulk alloys (such as Pt_3Sn (111)) indicated that surface alloy Sn atoms readily undergo surface segregation, leading to uneven active site distribution, while bulk alloy Sn atom distributions are more stable with superior catalytic performance.[25] Additionally, Sn modulation of Pt surface adsorption behavior was clearly demonstrated through DFT: propane remains weakly physisorbed on PtSn alloy surfaces, while propylene chemisorption strength significantly weakens, with adsorption mode transitioning from di-σ adsorption on Pt (111) surfaces to π adsorption on PtSn alloy surfaces [Fig. 4(a)-(c)], reducing further propylene reactions.[20]

2.1.3 PtIn Alloy Catalysts

Indium (In) as an emerging Pt-based alloying element forms single-atom alloys (SAA) with Pt that exhibit excellent PDH stability and selectivity under low Pt loadings, with DFT calculations revealing unique catalytic mechanisms.[1] In Pt-In SAA, individual Pt atoms are dispersed on In nanoparticle surfaces, with In introduction disrupting Pt-Pt bonds to form isolated Pt active sites, both increasing active site numbers and suppressing side reactions such as C-C bond cleavage. Electronic structure analysis shows that In transfers electrons to Pt, upshifting Pt d-band centers, enhancing C-H bond activation capability while weakening propylene adsorption strength. Propylene desorption barriers decrease by 0.3-0.5 eV [Fig. 4(d)-(e)] while deep dehydrogenation barriers increase by 0.2-0.4 eV, achieving propylene formation rates of 16.9 $mol \cdot g^{-1}Pt \cdot h^{-1}$ and low deactivation rates of 0.001 h^{-1} at 550°C.[1]

DFT calculations also optimized Pt-In alloy composition ratios, finding that when In loading is 1.5 w.t.% and Pt loading only 0.1 w.t.%, Pt-In interactions are strongest, forming the most stable single-atom dispersion structures. Excess In covers Pt active sites, causing activity decline.[1] Additionally, anti-coking performance of Pt-In alloys was explained through DFT: isolated Pt sites reduce adsorption and polymerization of coking precursors (such as propyne), and In-modified Pt surfaces increase coking adsorption energy by 0.4-0.6 eV, suppressing carbon deposition.[1]

2.1.4 Other Platinum-Based Alloy Catalysts

Beyond Sn and In, alloys or composite systems formed by Pt with elements such as Ga, Bi, B, Zn, and Ti have also been confirmed through DFT calculations to possess potential PDH application value. For Pt-Ga alloys, DFT calculations indicate that the Pt_3Ga (111) surface undergoes reconstruction due to Ga introduction, with significantly enhanced propane adsorption energy (-0.47 eV), while propylene desorption barriers decrease, rendering PDH activity superior to pure Pt.[12] In Pt-Ga single-atom alloys, isolated Pt sites can suppress deep dehydrogenation, achieving propylene selectivity as high as 94 %.[1] For Pt-Zn alloys, through DFT calculations combined with experimental characterization, the Pt-ZnO_x interface (structure: $Pt^{\delta+}$-Zn^{2+}-O-Si) was revealed as the PDH active site, where low-coordination Zn site-anchored Pt clusters reduce propane C-H bond activation barriers to 1.09 eV (far below 1.90 eV for Pt (111) surfaces), while simultaneously suppressing deep dehydrogenation, with propylene selectivity exceeding 99 %.[26] Additionally, [$PtZn_4$] single-center intermetallic compounds were confirmed to break adsorption energy scaling relationships through geometric isolation and electronic modulation, achieving synergistic

enhancement of activity and selectivity. For Pt-Ti composite systems, through DFT calculations combined with multiple characterization techniques, Ti doping was revealed to suppress PtZn nanoparticle sintering via strong Pt-Ti interactions, with Ti^{3+} sites transferring electrons to Pt^0 to form $Pt^{\delta-}$-Ti^{4+} systems, reducing CO adsorption strength and inducing infrared spectral red shifts, resulting in lower deactivation rates for $PtZnTi/SiO_2$ ($k_d=0.015\ h^{-1}$) compared to $PtZn/SiO_2$ ($k_d=0.022\ h^{-1}$), while maintaining stable catalytic performance after regeneration.[27] For Pt-Bi alloys, DFT results show that Bi introduction can maximize propylene selectivity enhancement ($\Delta E=0.97$ eV), but significantly reduces PDH activity, requiring optimization through particle size reduction and exposure of more low-coordination sites.[12] In boron (B)-doped $PtSnK-B/Al_2O_3$ catalysts, DFT calculations revealed that B forms stable Pt-B clusters with Pt, enhancing binding energy with the support (from -7.40 eV to -11.16 eV) [Fig. 4(f)], suppressing Pt sintering. Simultaneously, propane adsorption increases Pt-Pt bond lengths, promoting Pt atom dispersion, enabling the catalyst to achieve a single-pass lifetime of 310 h at 0.15 w.t.% low Pt loading, three times that of undoped catalysts.[2] Furthermore, DFT studies of Pt-Cu and other alloys also demonstrate that alloying elements can break adsorption energy scaling relationships by modulating Pt electronic structure (d-band center) and geometric structure (active site isolation), achieving synergistic enhancement of activity and selectivity.[12]

2.1.5 Platinum-Based Core-Shell Catalysts

In propane dehydrogenation coupled with selective oxidation systems, Pt-based core-shell catalysts exhibit unique advantages. Through DFT calculations and microkinetic simulations, the performance of 11 M@Pt (M=Fe, Co, Ni, Cu, Ru, Rh, Os, Ir, Pd, Ag, Au) core-shell catalysts was investigated, revealing that the O_2 dissociation pathway dominates hydrogen oxidation, with O_2 dissociation as the rate-controlling step, and propyne as the initial intermediate for C3 species oxidation.[28] Among these, Ag@Pt core-shell catalysts exhibited optimal performance, possessing both high hydrogen oxidation activity (H_2 conversion rate of 4.27 %) and the ability to weaken propylene adsorption through modulation of Pt surface electronic structure (d-band center upshift), suppressing oxidative consumption of propylene and demonstrating excellent propylene selectivity, making it the best candidate catalyst for selective hydrogen oxidation in coupled systems.

2.1.6 Summary of DFT Research on Platinum-Based Catalysts

DFT calculations have demonstrated powerful theoretical guidance in PDH research of Pt-based catalysts: through electronic structure analysis (d-band center, charge transfer), the modification mechanisms of alloying elements and dopant atoms have been revealed; through reaction pathway calculations, mechanistic differences among different crystal facets, sizes, and active sites have been clarified; through adsorption energy and barrier calculations, optimal alloy compositions, core-shell structures, and doping ratios have been screened; through integration with Bayesian statistics and microkinetic simulations, active sites and reaction kinetic patterns have been quantified. Future DFT research on Pt-based catalysts should focus on: synergistic effects in multi-component alloys, metal-support interactions in supported catalysts, dynamic evolution processes of carbon formation, and integration of DFT calculations with machine learning to provide more comprehensive theoretical support for rational design of industrial-grade catalysts.

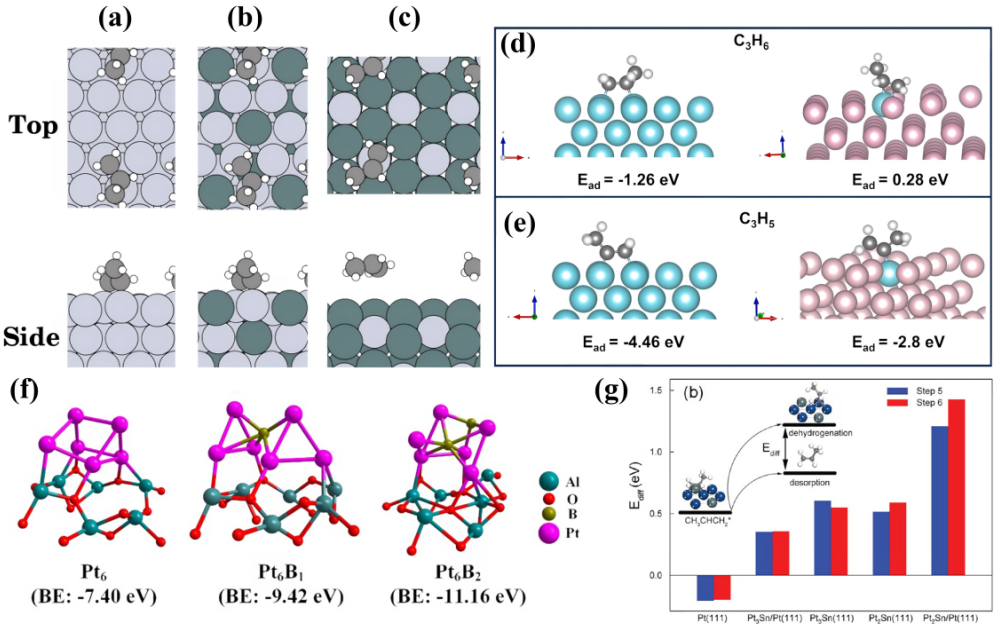

Figure 4. Propene adsorption geometries on (a) Pt(111), (b) Pt_3Sn-(111), and (c) $PtSn_2$ at 0.13 ML coverage. Pt atoms are colored light gray and Sn atoms green, whereas dark gray stands for C and white for H. Structures and adsorption energies of the adsorbates C_3H_6 (d) and C_3H_5 (e) on Pt NPs and Pt–In SAA models..(f) Optimized lowest-energy cluster structures of pure Pt_6,Pt_6B_1, and Pt_6B_2 and their corresponding binding energy on θ-Al_2O_3 (010). Note: For simplicity, K and Sn atoms were hided. (g) energy barrier difference (Ediff) between propylene dehydrogenation and propylene desorption over the Pt(111) and PtSn surfaces.

2.2 Chromium-Based Catalysts

Chromium-based catalysts (primarily Cr_2O_3 and CrO_x) have found widespread application in propane dehydrogenation (PDH) reactions due to their low cost and high activity, with catalytic performance closely related to active site structure, electronic properties, and reaction environment. Density functional theory (DFT) calculations have deeply revealed structure-performance relationships, reaction mechanisms, and modification mechanisms of chromium-based catalysts, providing critical theoretical support for rational catalyst design.

2.2.1 Pure Chromium Oxide Catalysts

The active sites of pure chromium oxide catalysts are mainly coordinatively unsaturated Cr^{3+} ions and surface Cr-O ion pairs, with PDH performance closely related to crystal facet structure and oxygen vacancy distribution. DFT studies indicate that the α-Cr_2O_3(0001) surface is the primary exposed crystal facet for PDH reactions, existing in both Cr-terminated and O-terminated configurations, with Cr-terminated surfaces being more stable and exhibiting higher activity.[29] The reaction follows a heterolytic C-H bond activation mechanism: C atoms in propane molecules adsorb at Cr sites, while H atoms preferentially bind with adjacent O sites, with Cr-O ion pairs cooperatively breaking C-H bonds to generate Cr-propyl and O-H intermediates.[30] Oxygen vacancies significantly influence the catalytic performance of pure chromium oxides. DFT calculations show that after removing lattice oxygen from α-Cr_2O_3 surfaces, electrons transfer to surrounding Cr atoms, raising Cr 3d orbital Fermi levels [Fig. 5(d)-(e)] and enhancing orbital interactions with adsorbates, thereby reducing C-H bond activation barriers. Simultaneously, oxygen vacancies alter surface Lewis acid-base properties, weakening Cr-O interactions with deep dehydrogenation products and suppressing side reactions. Surface oxidation states significantly modulate catalytic mechanisms and selectivity: reduced α-Cr_2O_3(0001) surfaces produce propylene through non-oxidative dehydrogenation pathways with selectivity as high as 99%; oxidized surfaces follow the Mars-van Krevelen mechanism, where H atoms combine with surface oxygen to generate H_2O, but readily trigger C-C bond cleavage to produce CO_2, with significantly reduced selectivity.[31] DFT combined with kinetic Monte Carlo (KMC)

simulations confirmed the existence of optimal surface oxidation degrees (0.2 when using O_2, 0.5 for N_2O), at which propylene yield is maximized.[31]

2.2.2 Single-Atom Doped Modified Chromium-Based Catalysts

Single-atom doping (such as Pt, Al) represents an effective strategy for optimizing chromium-based catalyst performance, with DFT calculations revealing electronic modulation and structural optimization mechanisms of dopant atoms. Platinum (Pt) single-atom doping can significantly enhance PDH activity and selectivity of Cr_2O_3. DFT research indicates that Pt single atoms preferentially occupy Cr vacancies on Cr_2O_3(0001) surfaces, forming strong interactions with adjacent O atoms, reducing the conduction band minimum (CBM) of O sites through charge transfer, enhancing H capture capability, and lowering the first-step dehydrogenation barrier of propane from 1.40 eV for pure Cr_2O_3 to 1.13 eV [Fig. 5(a)-(c)]. [32] Meanwhile, Pt single atoms modulate Cr-O Lewis acid-base interactions, raising deep dehydrogenation barriers (from 0.83 eV to 1.94 eV), suppressing carbon precursor formation, with propylene selectivity exceeding 92 %. Furthermore, Pt single atoms maintain atomic-level dispersion under both reaction and regeneration conditions, thermodynamically suppressing sintering agglomeration and enhancing catalyst stability. Aluminum (Al) doping optimizes PDH performance by altering Cr_2O_3 electronic structure and surface adsorption characteristics. DFT calculations show that after Al atoms dope into Cr_2O_3 lattices, electronegativity differences cause surface Cr^{6+} to convert to Cr^{3+}, increasing active site numbers. Simultaneously, Al doping reduces propylene adsorption energy (from -1.51 eV to -1.33 eV), promoting product desorption, while raising carbon formation barriers by 0.3-0.5 eV, significantly suppressing carbon deposition and extending catalyst lifetime. [33]

2.2.3 Composite Chromium-Based Catalysts

Composite chromium-based catalysts (such as Cr-Zr, Cr-Al composite oxides) optimize active site structures through synergistic effects between components, with DFT calculations clarifying synergistic mechanisms and reaction advantages. In Cr-Zr composite oxides, synergistic effects between ZrO_2 and CrO_x significantly enhance PDH performance. DFT research indicates that Zr atom introduction promotes CrO_x species dispersion, forming stable Cr-Zr-O active sites, where coordinatively unsaturated Zr (Zr_cus) cooperates with adjacent Cr sites to activate C-H bonds. [34] Calculations show that after Cr^{3+} doping into ZrO_2 lattices, oxygen vacancy formation energy decreases (from 5.45 eV to 2.39 eV), enhancing surface electron transport capability and reducing total propane dehydrogenation barriers from 1.13 eV for pure ZrO_2 to 0.95 eV.[34] Additionally, ZrO_2 presence weakens Cr-O interactions with propylene, suppressing deep dehydrogenation, with propylene selectivity reaching above 90 %.[33] In MIL-101 (Cr/Al)-derived Cr-Al composite oxide catalysts, DFT calculations revealed that Al introduction modulates Cr-O bond strength, optimizing surface acid site distribution. PDH reactions on this catalyst follow a two-step dehydrogenation mechanism: first-step C-H bond activation barrier is 1.79 eV, generating Cr-propyl intermediates; second-step dehydrogenation barrier decreases to 1.60 eV, producing propylene. Compared to pure Cr_2O_3, Al presence in composite catalysts raises adsorption energy of carbon precursors (propyne) by 0.4 eV, suppressing C-C bond cleavage and polymerization, with significantly enhanced anti-coking performance. [33]

2.2.4 Reaction Mechanisms and Side Reaction Control in Chromium-Based Catalysts

DFT calculations have clarified core reaction pathways and side reaction suppression mechanisms for PDH on chromium-based catalysts, providing theoretical basis for performance optimization. Regarding core reaction mechanisms, the rate-controlling step for PDH reactions on chromium-based catalysts is the first-step heterolytic C-H bond activation.[30] Taking Cr(III)-O sites as examples, DFT calculations show that these sites heterolytically cleave C-H bonds through σ-bond metathesis-type transition states, with methylene C-H bonds in propane preferentially activated (barrier 1.25-1.40 eV), generating propyl intermediates that further dehydrogenate to produce propylene (barrier 0.89-1.47 eV), with relatively low propylene desorption barriers (0.45-0.65 eV) ensuring rapid product desorption. [30] For side reaction control, carbon formation and deep dehydrogenation represent major challenges. DFT research indicates that strong Lewis acid sites on chromium-based catalyst surfaces readily adsorb propylene and trigger deep dehydrogenation, generating carbon precursors such as propyne. [31] By introducing oxygen vacancies or doping with Pt, Al, and other atoms, surface acidity strength can be reduced, weakening adsorption of deep dehydrogenation products and raising carbon formation barriers by 0.2-0.6 eV.[29] Additionally, oxidative

atmospheres exacerbate C-C bond cleavage to generate CO_2, while selecting N_2O as a mild oxidant can reduce CO_2 generation and carbon deposition while maintaining activity. [31]

2.2.5 Summary of DFT Research on Chromium-Based Catalysts

DFT calculations play a critical role in PDH research of chromium-based catalysts: clarifying Cr^{3+}, Cr-O ion pairs, and oxygen vacancies as core active sites, revealing heterolytic C-H bond activation reaction mechanisms, and elucidating synergistic mechanisms of single-atom doping and composite modification. Future research should focus on: electronic synergistic effects in multi-component doping, metal-support interactions in supported catalysts, dynamic evolution of carbon formation during reaction processes, and integration of DFT with microkinetic simulations and machine learning to provide more comprehensive theoretical support for developing high-activity, high-selectivity, long-lifetime chromium-based PDH catalysts.

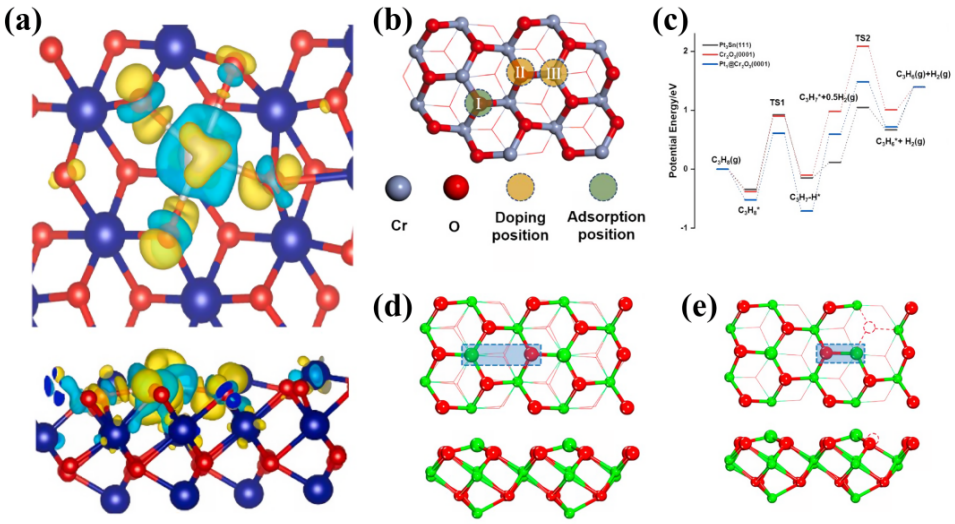

Figure 5. (a) Charge density difference of $Pt_1@Cr_2O_3(0001)$.(b) Pt atom position of Cr_2O_3 (0001). (c) Energy profiles for main reaction pathway towards propylene of PDH on $Pt_3Sn(111)$, Cr_2O_3 (0001) and $Pt_1@Cr_2O_3$ (0001). Top and side views of (d) Cr_2O_3 (0001), (e) oxygen-deficient Cr_2O_3 (0001). The ion pairs shaded are active sites on the respective surfaces.

2.3 Vanadium-Based Catalysts

Vanadium-based catalysts (primarily VO_x and V_2O_5) demonstrate broad application prospects in propane dehydrogenation (PDH) and oxidative dehydrogenation (ODH) reactions due to their tunable oxidation states, diverse active site structures, and excellent thermal stability. Density functional theory (DFT) calculations have deeply revealed the nature of active sites, reaction mechanisms, and modification mechanisms, providing critical theoretical support for catalyst performance optimization.

2.3.1 Pure Vanadium Oxide Catalysts

The catalytic performance of pure vanadium oxides is closely related to crystal facet structure, oxidation state, and surface oxygen species, with DFT calculations clarifying structure-performance relationships between active sites and reaction pathways. As a typical pure vanadium oxide, V_2O_5 exhibits significant activity differences among crystal facets. The $V_2O_5(001)$ surface contains two key sites: terminal oxygen O(1) and bridge oxygen O(2), where O(2) sites demonstrate superior propylene selectivity (exceeding 90 %) due to their combined C-H bond activation capability and low deep oxidation activity.[35] The reaction follows the Mars-van Krevelen mechanism: methylene C-H bonds in propane are preferentially activated (barrier 1.18 eV), generating isopropoxy intermediates that further dehydrogenate to produce propylene (barrier 0.96 eV). [36] Reaction pathways on $V_2O_5(010)$ surfaces depend on synergistic effects of dual V=O

groups: one V=O attacks the β-C atom of propane to form V-$OCH_2(CH_3)_2$ species, while another V=O converts to V-OH, with isopropoxy formation barriers (9.4 kcal/mol) significantly lower than n-propoxy (14.5 kcal/mol), offering both thermodynamic and kinetic advantages. The second dehydrogenation step requires O(3)H hydroxyl assistance, generating propylene and water through cooperative methyl hydrogen transfer with barriers around 15 kcal/mol, representing the rate-controlling step. Surface oxidation states and oxygen vacancies modulate catalytic performance: reduced V_2O_5 surfaces primarily undergo non-oxidative dehydrogenation pathways with propylene selectivity approaching 99%; oxidized surfaces readily trigger C-C bond cleavage to generate CO_2, with significantly reduced selectivity. DFT calculations indicate that oxygen vacancy formation energies vary with crystal facets and oxidation states, with V_2O_5(001) surface oxygen vacancy formation energy of 2.39 eV, enhancing orbital interactions between V sites and adsorbates through electron transfer, reducing C-H bond activation barriers. [37]

2.3.2 Supported Vanadium-Based Catalysts

Supports modulate vanadium species dispersion, oxidation state, and electronic properties through metal-support interactions (MSI), with DFT calculations revealing modulation mechanisms and optimal support systems for different supports. In CeO_2-supported VO_3 catalysts, the VO_3/CeO_2(111) surface contains three active oxygen species (O_V=O, O_V-O-Ce, O_Ce-O-Ce), where O_V-O-Ce and O_Ce-O-Ce synergistically achieve dissociative adsorption of propane (adsorption energy 3.08 eV).[36] A unique new localized empty state (NELS) composed of O 2p orbitals of VO_3 significantly reduces the first C-H bond breaking barrier (0.12 eV), while NELS occupation raises the second C-H bond breaking barrier to 1.81 eV, effectively suppressing deep dehydrogenation. [36] In SSZ-13 zeolite-supported VO_x catalysts, VO_3 (V^{3+}) species exhibit significantly superior activity to VO_4 (V^{5+}): VO_3 V-O-S sites serve as single active centers with first C-H bond breaking barriers of only 2.4-2.5 eV, while VO_4 exhibits barriers as high as 3.0-3.4 eV due to coordination crowding at V sites. [38] DFT combined with microkinetic simulations confirmed that propylene turnover frequency (TOF) of VO_3/SSZ-13 at 600°C reaches 0.37 s^{-1}, far exceeding VO_4/SSZ-13 (approaching 0). ZrO_2 supports optimize VO_x electronic structure through weak MSI: bridge oxygen in VO_x/ZrO_2 exhibits low electron density with C-H bond breaking barriers of only 1.10 eV, exhibiting activity over 4 times higher than VO_x/Al_2O_3. [39] DFT calculations indicate that the weak electron donor characteristics of ZrO_2 weaken V-O bond strength, promoting oxygen species migration while suppressing VO_x polymerization and enhancing active site dispersion. [39]

2.3.3 Modified Vanadium-Based Catalysts

Modification strategies such as doping and oxidant regulation can optimize activity, selectivity, and stability of vanadium-based catalysts, with DFT calculations revealing modification mechanisms and performance enhancement patterns. MgO doping significantly improves CO_2-assisted ODH performance of $VO_x@ZrO_2$: MgO reduces oxygen vacancy formation energy (from 31.1 eV to 3.91 eV), enhancing CO_2 adsorption and activation capability while extending spillover distances for H, O, and CO_2 intermediates, improving surface reaction kinetics. DFT simulations show that propane adsorption barriers for Mg-VZ catalysts decrease from 85.6 eV to 25.0 eV, ODH reaction barriers decrease from 94.1 eV to 39.2 eV, achieving propane conversion of 20.4% and propylene yield of 14.6% at 550°C. [37] Sulfur (S_2) as an alternative oxidant significantly enhances propylene selectivity: in S-V/SiO_2 catalysts, although sulfided surfaces exhibit propylene adsorption energies similar to oxidized surfaces, deep dehydrogenation barriers increase by 0.5-0.8 eV, suppressing CS_2 generation. DFT calculations indicate that propane C-H bond activation barriers on sulfided surfaces (111 kJ/mol) are higher than oxidized surfaces, but propylene selectivity reaches 96% with yields of 41%, far exceeding traditional O_2-ODH systems. [40]

2.3.4 Reaction Mechanisms and Side Reaction Control in Vanadium-Based Catalysts

DFT calculations have clarified core mechanisms and side reaction suppression pathways for PDH/ODH on vanadium-based catalysts, providing theoretical basis for selectivity optimization. Regarding core reaction mechanisms, PDH reactions follow two-step dehydrogenation mechanisms: the first step involves heterolytic activation of methylene or methyl C-H bonds (rate-controlling step), generating alkyl intermediates; the second step involves further dehydrogenation of intermediates to produce propylene, with relatively low desorption barriers (0.45-0.65 eV).[30] ODH reactions depend on lattice oxygen participation, following the Mars-van Krevelen mechanism, with lattice oxygen regenerated through oxidants (O_2, CO_2, S_2) after consumption. For side reaction control, deep oxidation and carbon formation

represent major challenges sites on $V_2O_5(001)$ surfaces readily trigger deep oxidation of propylene to generate acetone, acrylic acid, and CO_x, while O(2) sites remain inert toward deep oxidation; selectivity can be enhanced by regulating O(1)/O(2) ratios. [35] DFT research indicates that through support modification (such as ZrO_2, SiO_2) to weaken MSI, introduction of oxygen vacancies, or selection of mild oxidants (CO_2, S_2), C-H bond activation selectivity can be enhanced while reducing adsorption energy of carbon precursors (propyne, coke), suppressing side reactions. [40]

2.3.5 Summary of DFT Research on Vanadium-Based Catalysts

DFT calculations play a critical role in PDH/ODH research of vanadium-based catalysts: clarifying terminal oxygen, bridge oxygen, and V-O-support sites as core active centers, revealing heterolytic C-H bond activation and Mars-van Krevelen reaction mechanisms, and elucidating synergistic mechanisms of support modulation, doping modification, and oxidant optimization. Future research should focus on: electronic synergistic effects in multi-component doping, dynamic MSI evolution in supported catalysts, dynamic evolution of oxygen vacancies and carbon formation during reaction processes, and integration of DFT with microkinetic simulations and machine learning to provide more comprehensive theoretical support for developing high-activity, high-selectivity, long-lifetime vanadium-based dehydrogenation catalysts.

2.4 Gallium-Based Catalysts

Gallium-based catalysts—including Ga_2O_3, Ga-ZSM-5, Ga-CHA, and Ga alloys—exhibit outstanding performance in propane dehydrogenation (PDH) owing to their unique electronic structures, tunable types of active sites, and excellent selectivity. Density functional theory (DFT) calculations have been instrumental in revealing the nature of active sites, reaction mechanisms, and performance optimization strategies across these diverse gallium-containing catalyst architectures.

2.4.1 Pure Gallium Oxide Catalysts

Active Site Structure and Reaction Mechanism

Pure gallium oxide (Ga_2O_3) exhibits catalytic performance highly dependent on crystal facet structure, active site type, and reaction atmosphere. DFT calculations have identified the key structure-activity relationships and dehydrogenation pathways.

The thermodynamically stable and catalytically optimal β-$Ga_2O_3(100)$ surface contains two critical active site types: two-coordinated oxygen sites O(2) and unsaturated gallium sites Ga(o). Initial C-H bond activation predominantly follows a radical mechanism: the O(2) site abstracts a hydrogen atom from the propane methylene group, forming propyl radicals and hydroxyl groups (O(2)H) with an activation barrier of only 18.1 kcal/mol—significantly lower than the O(3) site (39.4 kcal/mol), establishing it as the core site for initial activation. Propyl radicals can subsequently generate propylene through two pathways: (1) hydrogen abstraction by adjacent O(2) sites (barrier 4.5 kcal/mol), or (2) coupling with Ga(o) sites to form propyl-gallium intermediates followed by dehydrogenation (barrier 29.6 kcal/mol).

Hydrogen Species Desorption Mechanism

The hydrogen species desorption mechanism determines catalytic cycle efficiency. DFT calculations reveal that the combination of surface GaH with hydroxyl groups (O(2)H/O(3)H) to form H_2 requires barriers of only 9.5-14.7 kcal/mol, representing the primary desorption pathway. In contrast, hydroxyl coupling to generate H_2O exhibits a higher barrier (20.3 kcal/mol), and H_2O desorption energy (>13 kcal/mol) significantly exceeds that of H_2 (<1 kcal/mol), indicating that direct dehydrogenation (DDH) mechanism dominates. However, under high temperatures or in the presence of mild oxidants like CO_2, the H_2O generation pathway becomes non-negligible, leading to surface oxygen vacancy formation that requires regeneration through oxidants to maintain activity.

Surface Ga-H Species as Key Intermediates

Surface Ga-H species serve as critical intermediates. On the α-Ga_2O_3 surface, H_2 heterolytic dissociation forms tetrahedral-coordinated [$HGaO_3$] structures (Ga-H bond length 1.56 Å), with DFT-calculated ^1H chemical shifts and quadrupolar coupling constants (CQ) showing excellent agreement with solid-state NMR experimental results.[41] These Ga-H species can undergo nucleophilic reactions with CO_2 to form formate intermediates, providing active species for subsequent hydrogenation to methanol. [41]

2.4.2 Zeolite-Supported Gallium Catalysts

Active Species Modulation through Confinement Effects

Zeolites (ZSM-5, CHA, etc.) modulate gallium species dispersion and electronic properties through pore confinement effects and metal-support interactions, with DFT calculations revealing active site characteristics and reaction mechanisms.

In Ga-ZSM-5 catalysts, gallium species exist primarily in two forms: isolated Ga^+ sites and $Ga_2O_2^{2+}$ species stabilized by paired Al atoms. DFT calculations demonstrate that $Ga_2O_2^{2+}$ sites exhibit C-H bond activation barriers (2.4-2.5 eV) significantly lower than isolated Ga^+ (3.0-3.4 eV), achieving turnover frequencies (TOF) of 0.37 s^{-1} at 600°C, making them highly efficient active centers. [38] The reaction follows a Lewis-Brønsted acid pair cooperative mechanism: Brønsted acid sites polarize propane C-H bonds while Lewis acid sites (Ga^{3+}) abstract hydrogen atoms to form Ga-H intermediates, subsequently releasing propylene.

In Ga-CHA molecular sieves, reduced extra-framework Ga^+ sites constitute the core active centers. DFT calculations show that Ga^+ reacts with H_2 to generate GaH_x species (formation enthalpy -34.0 kJ/mol), closely matching experimental values (-51.2 kJ/mol). The propane dehydrogenation barrier for Ga^+ sites (75.9-115 kJ/mol) is substantially lower than CHA zeolite's inherent acid-catalyzed barrier (159-200 kJ/mol), with propylene selectivity reaching 96%. Compared to In-CHA, Ga^+ exhibits stronger transition state stabilization, reducing C-H activation temperatures by 80-100°C and achieving TOF values 43 times higher than In^+ sites. [43]

2.4.3 Gallium-Based Alloy Catalysts

Electronic Transfer and Site Isolation Effects

Gallium alloys with noble metals (Pt, Rh) enhance PDH activity and stability through electronic transfer and site isolation effects, with DFT calculations elucidating interfacial interaction mechanisms and active site nature.

In Ga-Pt alloy (SCALMS system), Pt atoms are atomically dispersed in liquid Ga matrix. DFT simulations reveal Pt atoms dynamically migrate within liquid Ga, stabilizing at surfaces when adsorbing reactants, forming negatively charged Pt species (charge -0.68~-1.06 e) that significantly enhance C-H bond activation capability. [43] Propane dehydrogenation follows a cooperative mechanism: Pt sites activate C-H bonds to generate propyl intermediates that subsequently migrate to the Ga matrix, while Pt sites catalyze hydrogen recombination to H_2. Propylene desorption barriers are markedly reduced, suppressing deep dehydrogenation and coking.[43] H_2 pretreatment reduces surface GaO_x passivation layers—DFT calculations show Ga_2O_3 reduction to metallic Ga exhibits lower barriers (1.3-2.25 eV/unit) than gaseous Ga_2O formation, exposing more active sites and increasing propane conversion from 10 % to 26 %. [44]

In Ga-Rh alloys, Rh single atoms dynamically appear at liquid Ga interfaces. DFT calculations indicate Rh atoms carry negative charge (-0.83 *e*) due to Ga's electron donor effect, with C-H bond activation barriers (1.42 eV) significantly lower than pure Rh catalysts (>2.0 eV). The reaction pathway involves: propane undergoes first dehydrogenation at Rh sites (barrier 1.42 eV), hydrogen atoms diffuse to adjacent Ga sites (barrier 0.66 eV), second dehydrogenation generates propylene (barrier 1.31 eV), and the Ga matrix reduces propylene adsorption strength while suppressing coking formation. When Ga/Rh ratio exceeds 80, the alloy becomes fully liquid with maximum Rh site isolation, achieving 92% propylene selectivity and significantly superior stability compared to solid alloys. [45]

2.4.4 Reaction Mechanisms and Performance Tuning

DFT calculations have clarified core PDH mechanisms and performance tuning pathways for gallium-based catalysts, providing theoretical foundations for catalyst optimization.

Core Reaction Mechanisms

PDH reactions follow a two-step dehydrogenation mechanism: (1) C-H bond heterolytic or homolytic activation (rate-determining step) generating alkyl intermediates and hydrogen species (Ga-H or hydroxyl groups); (2) intermediate dehydrogenation producing propylene with hydrogen species recombination/desorption completing the catalytic cycle. Oxidative dehydrogenation (ODH) pathways, requiring higher energy barriers (>25 kcal/mol), occur only minimally in the presence of oxidants.

Performance Tuning Strategies

Coking and active site deactivation represent primary challenges. DFT calculations demonstrate that introducing Si into Ga-ZSM-5 enhances gallium species dispersion, suppresses cluster aggregation, and reduces coking precursor adsorption energies. In Ga-Pt alloys, the liquid Ga matrix's high fluidity enables dynamic active site repair, reducing coking deposition—DFT simulations show coking adsorption energy on liquid Ga surfaces (-1.2 eV) is substantially lower than solid Pt (-2.8 eV).[43] Furthermore, optimizing zeolite Si/Al ratios can fine-tune Ga^+ site densities, with Ga/Al ratios of 0.7-1.0 achieving optimal activity; excessive ratios form low-activity GaO_x species. [42]

2.4.5 Summary of DFT Research on Gallium-Based Catalysts

DFT calculations have played pivotal roles in gallium-based catalyst PDH research by: (1) identifying O(2) sites, extra-framework Ga^+, and Ga-Pt/Rh single-atom sites as core active centers; (2) revealing radical mechanisms, acid pair cooperative mechanisms, and interfacial cooperative mechanisms; (3) elucidating support modulation, alloying, and pretreatment performance optimization mechanisms.

Future research should prioritize: (1) electronic synergistic effects in multi-component gallium catalysts; (2) dynamic evolution of Ga-H species and oxygen vacancies during reactions; (3) quantitative description of zeolite pore confinement effects; (4) integration of DFT with microkinetic simulations and machine learning to provide more comprehensive theoretical support for developing high-activity, high-selectivity, long-lifetime gallium-based dehydrogenation catalysts.

2.5 Zinc-Based Catalysts

Zinc-based catalysts, primarily comprising ZnO, Zn-MFI, Zn-Zr composite oxides, and Zn single-atom catalysts, have emerged as important alternative systems to Pt-based and Cr-based catalysts for propane dehydrogenation (PDH) reactions due to their abundant reserves, low cost, and environmental friendliness. Density functional theory (DFT) calculations have deeply revealed the nature of active sites, reaction mechanisms, and modification control mechanisms, providing crucial theoretical support for catalyst structure optimization and performance enhancement.

2.5.1 Pure Zinc Oxide and Supported Zinc Oxide Catalysts

Active Sites and Structure-Activity Relationships

The catalytic performance of pure ZnO and supported ZnO catalysts is closely related to active site dispersion, support interactions, and surface species states, with DFT calculations clarifying their structure-activity relationships and reaction pathways.

ZnO Nanoclusters as Core Active Centers: DFT calculations demonstrate that ZnO nanoclusters can exist stably on hydroxyl-poor Al_2O_3 supports, avoiding the formation of low-activity $ZnAl_2O_4$ spinel phase at high temperatures. In the ZnO/Al_2O_3 system, the C-H bond activation barrier for ZnO nanoclusters (1.40 eV) is significantly lower than that of $ZnAl_2O_4$ (1.96 eV), and propylene adsorption energy (-1.08 eV) is weaker, suppressing deep dehydrogenation and coking [Fig. 6(f)]. [6]

Support Surface Hydroxyl Control of Active Site Evolution: Hydroxyl groups on the Al_2O_3 surface reduce the migration barrier of Zn atoms (from 2.21 eV to 1.54 eV), promoting Zn diffusion into the support interior to form $ZnAl_2O_4$. By contrast, hydroxyl-poor A-Al_2O_3 supports prepared via sol-gel methods can inhibit $ZnAl_2O_4$ formation, enabling Zn species to exist stably as ZnO nanoclusters and significantly enhancing catalytic stability [Fig. 6(d)-(e)]. [6]

Reaction Mechanism Following Two-Step Dehydrogenation Pathway: DFT calculations show that propane first undergoes C-H bond heterolytic cleavage at Zn^{2+} sites on the ZnO surface, generating propyl intermediates (C_3H_7) and hydroxyl groups (Zn-OH) with a barrier of 1.24-1.40 eV. Subsequently, C_3H_7 undergoes further dehydrogenation to produce propylene, with hydrogen species recombining to H_2 and desorbing. Compared to $ZnAl_2O_4$, ZnO surfaces exhibit lower barriers for both dehydrogenation steps and easier propylene desorption, resulting in higher selectivity. [6]

2.5.2 Zeolite-Supported Zinc-Based Catalysts

Active Site Control Through Framework Incorporation and Confinement

Zeolites (Silicalite-1, ZSM-5, etc.) modulate the electronic properties and dispersion of Zn species through pore confinement effects and framework incorporation, with DFT calculations revealing active site characteristics and reaction mechanisms.

Active Site Regulation via Framework-Incorporated Zn Species: Zn atoms incorporated into Silicalite-1 framework T7 sites through isomorphous substitution exhibit the lowest energy, forming stable Zn-O-Si structures. [46] DFT calculations show that framework Zn^{2+} sites have C-H bond activation barriers (1.35 eV) significantly lower than non-framework Zn species, with pore confinement effects enhancing reactant adsorption and intermediate stabilization.

Pt-Zn Synergistic Effects for Performance Optimization: In atomically dispersed $Pt\delta^{+}$-O-Zn structures supported on Silicalite-1, Pt and Zn form strong electronic interactions through oxygen bridge linkages [Fig. 6(a)-(b)]. DFT calculations demonstrate that $Pt\delta^{+}$ sites reduce propane adsorption energy (-0.70 eV) and lower C-H bond activation barriers from 1.40 eV (pure Zn sites) to 1.34 eV, while simultaneously suppressing Pt sintering.

Anchoring Effects in Zinc Silicate Zeolites: In zinc silicate zeolites, O atoms in Si-OH-Zn groups exhibit strong anchoring effects on Co species, forming isolated $Co\text{-}O_4$ active sites. DFT calculations indicate that framework Zn modulates O atom 2p orbital energy [Fig. 6(c)], enhancing the locking effect on Co and reducing C-H bond activation barriers to below 1.0 eV, significantly improving PDH activity. [47]

2.5.3 Zinc-Based Composite Oxide Catalysts

Synergistic Catalysis Through Electronic Structure Modulation

Composite oxides formed by Zn with Zr, Al, and other elements regulate electronic structure and oxygen mobility through synergistic effects, with DFT calculations revealing their active site cooperation mechanisms and reaction pathways.

Synergistic Catalysis in Zn-Zr Composite Oxides: In $ZnZr_xO_\gamma$ composite oxides, the Zn(cus)-O-Zr(cus) structure serves as the core active site, where Zn(cus) is responsible for the first C-H bond activation (barrier 0.61 eV), and Zr(cus) catalyzes the second dehydrogenation (barrier 0.52 eV). DFT calculations show that Zn incorporation increases Zr-O bond length from 2.32 Å to 2.43 Å, weakening metal-oxygen interactions, enhancing oxygen mobility, and reducing overall reaction barriers.

Phase Structure and Crystal Size Effects: The tetragonal phase of ZrO_2 (t-ZrO_2) more easily forms oxygen vacancies and Zr(cus) sites compared to the monoclinic phase (m-ZrO_2). DFT calculations show that oxygen vacancy formation energy in t-ZrO_2 (-1.36 eV) is lower, with more significant synergistic effects upon Zn complexation. $ZnZr_2$ composite oxides exhibit optimal performance with 21 % propane conversion at 450°C and 92 % propylene selectivity, with DFT verification showing the lowest apparent activation energy (68 kJ/mol).[48]

2.5.4 Zinc-Based Single-Atom Catalysts

Performance Through Precise Coordination Environment Control

Zn single-atom catalysts (Zn_1/NC) achieve high activity and stability through precise coordination environment control, with DFT calculations clarifying coordination structures, electronic properties, and reaction mechanisms.

Coordination Environment Regulation of Catalytic Performance: The $Zn_1\text{-}N_2C_2$ structure represents the optimal coordination form for NC-supported Zn single-atom catalysts, with binding energy (-0.18 eV) significantly higher than $Zn_1\text{-}N_4$ (0.31 eV), avoiding Zn atom aggregation. DFT calculations demonstrate that $Zn_1\text{-}N_2C_2$ exhibits lower C-H bond activation barriers (1.89 eV) compared to $Zn_1\text{-}N_4$ (2.27 eV), with weaker propylene adsorption energy (-0.35 eV), enhancing selectivity.

Synergistic Regulation of Peripheral P Doping: P atom doping optimizes the electronic structure of $Zn_1\text{-}N_2C_2$, enhancing C site affinity for H (adsorption energy decreases from -0.32 eV to -0.79 eV), further reducing the first dehydrogenation barrier to 1.39 eV. Simultaneously, P doping stabilizes Zn's tetracoordinate structure, lowering the second dehydrogenation barrier to 0.51 eV while suppressing Zn^{2+} reduction to metallic Zn, improving catalytic stability.[49]

2.5.5 Reaction Mechanisms and Performance Regulation

Core Mechanisms and Tuning Strategies

DFT calculations have clarified the core PDH mechanisms and performance regulation pathways for zinc-based catalysts, providing theoretical foundations for catalyst optimization.

Core Reaction Mechanism: PDH reactions follow a two-step dehydrogenation mechanism: the first step involves C-H bond activation (rate-controlling step) generating alkyl intermediates and hydrogen species (Zn-OH or surface H*); the second step involves intermediate dehydrogenation producing propylene, with hydrogen species recombination and desorption completing the catalytic cycle.[6] Different zinc-based systems exhibit distinct active sites: pure ZnO primarily features Zn^{2+} sites, composite oxides contain Zn(cus)-O-Zr(cus) synergistic sites, and single-atom catalysts feature Zn_1-N_nC_{4-n} coordination sites.[48,49]

Performance Tuning Strategies: Coking and active site deactivation represent primary challenges. DFT calculations demonstrate that through support hydroxyl control (e.g., hydroxyl-poor Al_2O_3), composite metal doping (e.g., Zn-Zr), and single-atom coordination environment optimization (e.g., P doping), active site aggregation, spinel phase formation, and deep dehydrogenation can be suppressed. Additionally, optimizing zeolite Si/Zn ratios or composite oxide Zn/Zr ratios (e.g., $ZnZr_2$) can optimize active site density and electronic properties, enhancing catalytic activity and stability.[48]

2.5.6 Summary of DFT Research on Zinc-Based Catalysts

DFT calculations have played crucial roles in zinc-based catalyst PDH research by: (1) identifying ZnO nanoclusters, Zn(cus)-O-Zr(cus) synergistic sites, and Zn_1-N_2C_2 single-atom sites as core active centers; (2) revealing two-step dehydrogenation mechanisms and support/doping control mechanisms.

Future research should focus on: (1) electronic synergistic effects in multi-component composite zinc-based catalysts; (2) dynamic evolution of Zn species during reactions; (3) precise control of zeolite pore confinement and single-atom coordination environments; (4) integration of DFT with microkinetic simulations to provide more comprehensive theoretical support for developing high-activity, high-selectivity, long-lifetime zinc-based dehydrogenation catalysts.

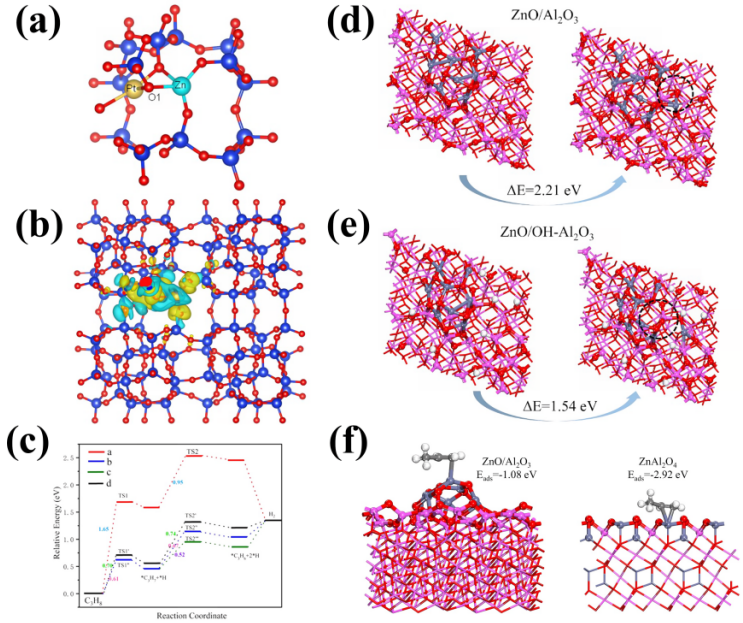

Figurer 6. Optimized structural models of $0.05Pt_2Zn$@S-1-FR (a) differential charge density on $0.05Pt_2Zn$@S-1-FR (b) where yellow and cyan represent the increase and decrease of chargedensity, respectively (c) Minimum-energy pathway for the C_3H_8 dehydrogenation on different sites of Zn−Zr catalysts. (d, e) DFT calculated formation energy of $ZnAl_2O_4$ spinel on ZnO/Al_2O_3 (without surface OH groups) and ZnO/OH- Al_2O_3 (with surface groups). (f) DRIFTS spectra of -OH groups.

2.6 Boron-Based and Boron-Nitrogen-Based Catalysts

Boron-based and boron-nitrogen-based catalysts (encompassing h-BN, BCN, BPO_4, boron carbides, and boron oxides) have emerged as research hotspots for propane dehydrogenation (PDH/ODHP) reactions due to their high olefin selectivity, metal-free characteristics, and tunable structures. Density functional theory

(DFT) calculations have deeply revealed the nature of active sites, reaction mechanisms, and structural regulation mechanisms, providing critical theoretical support for catalyst performance optimization.

2.6.1 Hexagonal Boron Nitride (h-BN) Catalysts

The catalytic performance of h-BN is closely related to edge defects, oxygen species modification, and active site types, with DFT calculations clarifying structure-activity relationships and reaction pathways.

Active Sites and Oxygen Species Regulation: The zigzag edges of h-BN (zigzag-BOH, zigzag-bri-B) constitute the core active regions for ODHP reactions, capable of in-situ generation of boron peroxide species (>B-O-O-B<, >B-O-OH) as mild oxidants.[50] DFT calculations demonstrate that boron peroxide species exhibit significantly higher selectivity for secondary C-H bond dehydrogenation in propane compared to primary C-H bonds, with isopropyl radical formation ratios (34.95) far exceeding n-propyl radicals (2.22), thereby suppressing deep oxidation.

Reaction Mechanism and Energy Barrier Characteristics: h-BN-catalyzed ODHP follows a three-step mechanism: "O_2 activation - propane dehydrogenation - propylene desorption." O_2 activation at boron hydroxyl sites (>B-OH) to generate ·OOH exhibits an energy barrier of 32.66 kcal/mol, while secondary C-H bond activation in propane requires only 13.56 kcal/mol. In h-BN/TS-1 heterostructures, interfacial charge transfer increases B atom charge from 0.288 to 0.297 while reducing excited state energy and enhancing electron mobility, achieving 8 % propane conversion and 62% propylene selectivity.[51]

2.6.2 Boron Carbon Nitride (BCN) Catalysts

BCN regulates electronic structure and active site density through carbon doping, with DFT calculations revealing the effects of carbon content and structural topology on catalytic performance.

Carbon Content and Activity Synergistic Effects: Appropriate carbon doping (7.7%-12.0%) enhances O-2p orbital electron density in BCN, reducing C-H bond activation barriers. The optimal system reduces propane dehydrogenation barriers from 2.30 eV (h-BN) to 1.06 eV. DFT calculations show that carbon doping optimizes H affinity by regulating metal-O binding energy (0.18-0.31 eV), matching O-H bond dissociation and regeneration rates to enhance low-temperature activity.[53]

Structural Reconstruction and Active Site Optimization: Through "carbon-oxygen replacement" strategies converting B-C_3 units in BCN to B-O_3 units, DFT verifies that B-O_3 sites preferentially adsorb propane and reduce C-H bond activation barriers, achieving 50.4% propane conversion and 32.7 % olefin yield.[54] Hierarchical BCN structures (such as 2D sheets wrapped with zigzag nanosheets) further enhance catalytic stability by increasing specific surface area (156.5 m^2/g) and exposing more active sites.[52]

2.6.3 Boron Phosphate (BPO_4) Catalysts

The catalytic performance of BPO_4 correlates with surface hydroxyl site types and P-B synergistic effects, with DFT calculations clarifying multi-active site cooperative mechanisms.

Active Site Types and Reaction Pathways: Three types of active sites exist on BPO_4 surfaces: tricoordinate boron hydroxyls (>B-OH), tetracoordinate boron hydroxyls (≡B-OH), and phosphate hydroxyls (≡P-OH). Tricoordinate boron sites exhibit the lowest C-H bond activation barrier (17.5 kcal/mol), while tetracoordinate phosphorus sites show weaker activity (28.7 kcal/mol). DFT calculations indicate that P elements regulate boron site electronic environments through B-O-P bridge bonds, making the rate-determining step barrier of BPO_4 (57.8 kcal/mol) higher than B_2O_3, resulting in slightly lower reactivity but superior selectivity.

Microenvironment and Water-Assisted Regulation: Surface hydroxyl coverage and spatial constraints in BPO_4 influence catalytic performance. Rigid microenvironments (crystalline lattice restrictions) reduce hydrogen bonding interactions, lowering O-H bond dissociation barriers (62.0 kcal/mol). Water molecules assist B-O-R species decomposition through hydrogen bonding networks, reducing barriers from 67.2 kcal/mol to 59.6 kcal/mol, promoting active site regeneration.[55]

2.6.4 Boron Carbide Catalysts

The catalytic performance of boron carbides ($B_{13}C_2$, B_4C, h-BC) depends on boron content and surface hydroxyl coverage, with DFT calculations revealing structure-activity correlations.

Boron Content and Electronic Structure Regulation: Higher boron content increases catalyst HOMO energy ($B_{13}C_2$: -5.876 eV; h-BC: -6.411 eV), enhancing electron delocalization and reducing C-H bond activation

barriers. DFT calculations show that $B_{13}C_2$-H (high hydroxyl coverage) exhibits secondary C-H bond activation barriers (8.2 kcal/mol) significantly lower than B_4C-H (15.0 kcal/mol) and h-BC (19.4 kcal/mol), demonstrating clear kinetic advantages.

Reaction Mechanism and Selectivity Control: Boron carbide-catalyzed ODHP follows an "O_2 activation - two-step dehydrogenation" mechanism, where surface >BO· species preferentially activate secondary C-H bonds. Generated isopropyl radicals undergo gas-phase ·OH or ·OOH-assisted dehydrogenation to form propylene, avoiding C-C bond cleavage. Non-covalent interaction (NCI) analysis indicates that high hydroxyl coverage surfaces stabilize transition states through O-H···O hydrogen bonds, further reducing reaction barriers.[56]

2.6.5 Boron Oxides and Composite Boron-Based Catalysts

Boron oxides (B_2O_3) and metal-promoted boron-based catalysts (BO_x/M/BN) enhance performance through active site synergy and electronic structure regulation, with DFT calculations clarifying regulatory mechanisms.

Anti-Deep Oxidation Characteristics of Boron Oxides: Support-free nanoscale B_2O_3 clusters can capture alkoxy radicals ($\cdot OC_3H_7$) with reaction barriers around 24 kcal/mol, suppressing CO_x formation. DFT calculations show that internal tricoordinate boron sites (Bi) in B_2O_3 clusters exhibit stronger alkoxy affinity than edge sites (Bt, Bm), with spin density primarily distributed on oxygen atoms, avoiding boron site deactivation.[57]

Metal Promotion and Alloy Regulation: In BO_x/Ni/BN catalysts, Ni regulates B-OH O-H bond dissociation/regeneration rates through metal-O binding energy (0.2-0.3 eV), achieving 22.5% propane conversion at low temperature (440°C). Ni-Rh alloys (15:1 molar ratio) further optimize metal-O binding energy, raising BO_x active site intrinsic activity to 9.26 μmol/(m^2·s), 105.9 times that of pure h-BN.[53]

2.6.6 Summary of DFT Research on Boron-Based and Boron-Nitrogen-Based Catalysts

DFT calculations have played a core role in boron-based and boron-nitrogen-based catalyst research: identifying B-O_3, boron peroxide species, and edge hydroxyl sites as core active centers; revealing the unique mechanism of "mild oxidation-selective dehydrogenation-anti-deep oxidation"; and confirming the effectiveness of regulation strategies including carbon doping, metal promotion, and heterostructure construction. Future research should focus on: multi-component synergistic effects (such as B-C-N-O quaternary systems), dynamic evolution of active sites during reactions, and multi-scale studies combining DFT with microkinetic simulations to provide more comprehensive theoretical support for developing high-activity, high-stability boron-based dehydrogenation catalysts.

2.7 Other Metal and Metal Oxide Catalysts

Beyond traditional precious metal and boron-based catalysts, non-precious metals such as Ni and Co, along with metal oxides like TiO_2 and ZrO_2, have become important research directions for propane dehydrogenation (PDH) catalysts due to their low cost, environmental friendliness, and structural tunability. Density functional theory (DFT) calculations have deeply revealed the nature of active sites, electronic structure regulation mechanisms, and reaction pathway differences, providing critical theoretical support for catalyst performance optimization.

2.7.1 Nickel (Ni)-Based Catalysts

Ni-based catalysts attract attention for their high C-H bond activation capability, but pure Ni readily undergoes deep dehydrogenation and coking. Alloying modifications have become the primary optimization strategy.

Active Sites and Electronic Structure Regulation: Introducing elements such as In, Zn, and Cu to form Ni-based intermetallic compounds (e.g., NiIn, NiZn) can significantly increase Ni atomic spacing (Δd), weakening Ni-C interactions.[58] DFT calculations show that Ni atomic spacing in NiIn alloys increases from 2.479 Å (pure Ni) to 3.177 Å, raising propylene deep dehydrogenation barriers from 0.8 eV to 1.2 eV, effectively suppressing side reactions.

Selectivity Descriptors and Structure-Activity Relationships: A "degree-of-isolation" descriptor has been proposed, integrating atomic radius, electronegativity difference, Ni atomic spacing, and electron shell number to quantitatively describe Ni-C repulsion. This descriptor exhibits a volcano-type relationship with

propylene selectivity. NiIn achieves theoretical propylene selectivity of 91 % due to moderate Ni-C repulsion, consistent with experimental results.

Reaction Mechanism Characteristics: Ni-based alloy-catalyzed PDH follows the isopropyl pathway ($CH_3CH_2CH_3 \rightarrow CH_3CHCH_3 \rightarrow CH_3CHCH_2$). Alloying shifts the rate-determining step (RDS) from C-H bond activation (0.9 eV barrier for pure Ni) to propylene desorption (1.0 eV barrier), enhancing selectivity. DFT calculations confirm that propylene adsorption energy on NiIn surfaces (-0.47 eV) is significantly lower than pure Ni (-1.2 eV), promoting product desorption.[58]

2.7.2 Cobalt (Co)-Based Catalysts

The crystal structure (HCP/FCC) of Co-based catalysts significantly impacts PDH performance, with DFT calculations clarifying structural sensitivity and reaction mechanisms.

Crystal Structure Effects: HCP-Co(0001) surface Co atoms have lower coordination numbers (9) compared to FCC-Co(111) (12), reducing C-H bond activation barriers by 0.2-0.3 eV. HCP-Co surface propylene adsorption energy (-0.58 eV) is weaker than FCC-Co (-0.72 eV), reducing deep dehydrogenation tendencies.[59]

Single-Atom and Support Effects: SiO_2-supported single-atom Co^{2+} catalyzes PDH through a non-redox mechanism. DFT calculations show C-H bond activation barriers (1.05 eV) lower than nano-Co particles (1.32 eV), with propylene selectivity reaching 92%. Electron transfer between Co and the support results in moderately positively charged Co^{2+}, optimizing intermediate adsorption strength and suppressing coking.

2.7.3 Titanium Dioxide (TiO_2) Catalysts

Defect engineering represents the core optimization strategy for TiO_2-catalyzed PDH, with oxygen vacancy (OV) formation and regulation directly affecting catalytic performance.

Active Site Nature: DFT calculations confirm that tetracoordinate Ti atoms (Ti^{4+}) surrounding TiO_2 surface oxygen vacancies constitute core active sites. OVs enhance Ti atom oxidizing properties, promoting propane adsorption and C-H bond activation. Perfect TiO_2(101) surface propane adsorption energy is only -0.028 eV, while defect surfaces with OVs increase adsorption energy to -0.155 eV, with dissociative adsorption barriers decreasing from 1.929 eV to 2.095 eV.

Defect Regulation and Stability: Hydrogen reduction regulates OV density in TiO_2. H_2-TiO_2-600 (reduced at 600°C) possesses optimal OV concentration, with PDH reaction barriers (1.8 eV) lower than air-treated samples (2.3 eV). DFT calculations show that excessive reduction temperatures (e.g., 700°C) cause Ti^{3+} overgeneration, weakening OV signals and decreasing catalytic activity.

Reaction Pathway Characteristics: Defective TiO_2-catalyzed PDH follows a "molecular adsorption - dissociative dehydrogenation - propylene desorption" mechanism. Tetracoordinate Ti atoms adsorb propane methyl groups, OV sites promote H atom migration, and propylene ultimately desorbs rapidly through weak adsorption, achieving selectivity above 85 %.[60]

2.7.4 Zirconium Dioxide (ZrO_2) Catalysts

ZrO_2 and Zr-based composite oxides (e.g., $LaZrO_x$, $YZrO_x$) achieve efficient PDH catalysis by regulating coordinatively unsaturated Zr sites (Zr^{3+}).

Active Sites and Synergistic Effects: DFT calculations show that dual Zr^{3+} sites adjacent to ZrO_2 surface oxygen vacancies serve as active centers, synergistically activating propane C-H bonds. La doping enhances oxygen vacancy stability in ZrO_2, increasing Zr^{3+} concentration by 30% and reducing C-H bond activation barriers from 1.2 eV to 0.9 eV.

Selectivity Control Mechanisms: ZrO_2 surface propylene adsorption energy (-0.6 eV) is significantly lower than Pt (-0.97 eV), with deep dehydrogenation barriers (1.5 eV) higher than propylene desorption barriers (1.1 eV), effectively suppressing side reactions. DFT calculations confirm that ZrO_2 oxygen vacancies weaken propylene-surface π-π interactions through electron transfer regulation, enhancing selectivity.

2.7.5 Other Metal and Metal Oxide Catalysts

Molybdenum Carbides (Mo_2C): β-Mo_2C(001) surface Mo atoms possess noble metal-like electronic structures. DFT calculations show C-H bond activation barriers (16.23 kcal/mol) lower than pure Pd (20.1 kcal/mol). After loading Pd or Cu single atoms, active site dispersion improves. Pd_1/Mo_2C RDS barriers

decrease to 8.53 kcal/mol, with deep dehydrogenation barriers (30.94 kcal/mol) significantly higher than propylene desorption barriers (24.34 kcal/mol).

Rhodium-Zirconium Composite Oxides ($RhZrO_2$): Strong interactions between Rh and ZrO_2 supports maintain Rh in highly dispersed states. DFT calculations show ZrO_2 surface oxygen vacancies transfer electrons to Rh, reducing C-H bond activation barriers from 1.0 eV (pure Rh) to 0.7 eV. Rh-Zr synergistic sites suppress propylene adsorption, achieving selectivity above 90 %.[61]

2.7.6 Summary and Outlook

DFT calculations have clarified core optimization directions in non-precious metal and metal oxide catalyst research: non-precious metals (Ni, Co) require alloying to regulate atomic spacing and electronic structure, suppressing deep dehydrogenation; metal oxides (TiO_2, ZrO_2) require defect engineering to construct coordinatively unsaturated metal sites, strengthening C-H bond activation and product desorption. Future research should focus on multi-component synergistic effects (such as metal-oxide interfacial effects), dynamic evolution of active sites during reactions, and multi-scale studies combining DFT with microkinetic simulations to provide theoretical support for developing low-cost, high-stability PDH catalysts.

References

[1] Lin, J.; Shen, M.; Zhang, C.; Bi, S.; Shen, G.; Gao, F.; Li, W. Active and stable platinum-indium single atom alloy catalysts for propane dehydrogenation. *Chemical Engineering Journal* **2025**, *519*. DOI: 10.1016/j.cej.2025.165243.

[2] Liu, M.; Han, S.; Zhang, W.; Gu, B.; Li, J.; Wei, H.; Rong, X.; Sun, C. Boron-Induced Redispersion of Pt Species during Propane Dehydrogenation. *ACS Catalysis* **2025**, *15* (5), 4251-4258. DOI: 10.1021/acscatal.4c07243.

[3] Lin, J.; Shen, M.; Bi, S.; Shen, G.; Gao, F.; Li, W. PtIn Alloy Supported on Y2O3-Modified δ-Al2O3 as a Propane Dehydrogenation Catalyst. *ACS Catalysis* **2025**, *15* (14), 12407-12419. DOI: 10.1021/acscatal.5c03103.

[4] Wang, S.-W.; He, Z.-H.; Tian, Y.; Zhu, Z.-J.; Sun, Y.-C.; Wang, K.; Wang, W.; Yang, Y.; Wang, H.; Liu, Z.-T. Photothermal catalytic CO2 oxidative dehydrogenation of propane over a dual functional Pt-GaN/SrTiO3 catalyst. *Applied Catalysis B: Environment and Energy* **2024**, *356*. DOI: 10.1016/j.apcatb.2024.124246.

[5] Kim, J.-S.; Chung, I.; Oh, J.; Park, J.; Yun, Y.; Shin, J.; Kim, H. W.; Chang, H. Closed-loop optimization of catalysts for oxidative propane dehydrogenation with CO2 using artificial intelligence. *Journal of CO2 Utilization* **2023**, *78*. DOI: 10.1016/j.jcou.2023.102620.

[6] Wang, Z.; Chen, H.; Song, S.; Liu, B.; Song, W.; Li, L.; Liu, J. Hydroxyl-Poor Al2O3 Avoids the Formation of ZnAl2O4 Spinel for Propane Dehydrogenation. *Industrial & Engineering Chemistry Research* **2024**, *63* (45), 19457-19465. DOI: 10.1021/acs.iecr.4c02389.

[7] Hao, X.; Zhao, X.; Zhou, Y.; Xu, Y.; Xia, J.; Wu, L.; Wei, T.; He, Z.-H.; Ma, S.; Xu, B. Boosting photothermal propane dehydrogenation via synergistic Co-Zr doping in CeO2 nanorods. *Molecular Catalysis* **2026**, *590*. DOI: 10.1016/j.mcat.2025.115634.

[8] Liu, X.; Yao, Z.; Lai, J.; Li, J.; Wang, J. Hydrogen coverage effects and structure sensitivity in propane dehydrogenation on Pt nanoparticles. *Chemical Engineering Science* **2026**, *319*. DOI: 10.1016/j.ces.2025.122299.

[9] Sun, S.; Sun, G.; Pei, C.; Zhao, Z.-J.; Gong, J. Origin of Performances of Pt/Cu Single-Atom Alloy Catalysts for Propane Dehydrogenation. *The Journal of Physical Chemistry C* **2021**, *125* (34), 18708-18716. DOI: 10.1021/acs.jpcc.1c04295.

[10] Xu, S.; Huang, Y.; Qie, M.; Yang, Y.; Wang, W.; Wu, K.; Li, W.; Li, Z.; Shen, Z.; Yang, H. Density functional theory study on propane dehydrogenation to propylene catalyzed by β-Mo2C(001)-based catalysts. *International Journal of Hydrogen Energy* **2025**, *179*. DOI: 10.1016/j.ijhydene.2025.151711.

[11] Feng, H.; Ge, Z.; Deng, Y.; Pu, P.; Zhao, S.; Song, X.; Yuan, H.; Wu, Y.; Yang, J.; Si, Y.; et al. Unveiling high-performance single-atom alloy catalysts for alkane dehydrogenation through DFT and machine learning synergy. *Journal of Catalysis* **2025**, *448*. DOI: 10.1016/j.jcat.2025.116213.

[12] Liang, K.; Zeng, X.; Ma, R.; Zou, G.; Dang, L.; Li, S. A theoretical investigation of propane dehydrogenation on Pt and Ni-based alloys. *Journal of Catalysis* **2023**, *428*. DOI: 10.1016/j.jcat.2023.115162.

[13] Cao, L.; Wei, F.; Chen, Y.; Pan, X.; Cao, H.; Su, Y.; Zhao, Y.; Chen, D.; Chai, Y.; Chen, L.; et al. Atomic Coordination Editing Achieves Ultraproductive Single-Atom Catalysts with Ultralow Loadings. *Journal of the American Chemical Society* **2025**, *147* (42), 38752-38761. DOI: 10.1021/jacs.5c14188.

[14] Salom-Català, A.; Strugovshchikov, E.; Kaźmierczak, K.; Curulla-Ferré, D.; Ricart, J. M.; Carbó, J. J. Reactive Force Field Development for Propane Dehydrogenation on Platinum Surfaces. *The Journal of Physical Chemistry C* **2024**, *128* (7), 2844-2855. DOI: 10.1021/acs.jpcc.3c07126.

[15] Liu, Z.; Lu, A.-H.; Wang, D. Deep Potential Molecular Dynamics Study of Propane Oxidative Dehydrogenation. *The Journal of Physical Chemistry A* **2024**, *128* (9), 1656-1664. DOI: 10.1021/acs.jpca.3c07859.

[16] Xiao, L.; Shan, Y.-L.; Sui, Z.-J.; Chen, D.; Zhou, X.-G.; Yuan, W.-K.; Zhu, Y.-A. Beyond the Reverse Horiuti–Polanyi Mechanism in Propane Dehydrogenation over Pt Catalysts. *ACS Catalysis* **2020**, *10* (24), 14887-14902. DOI: 10.1021/acscatal.0c03381.

[17] Pan, J.; Bru, G.; Carbó, J. J.; Godard, C.; Ricart, J. M. Propane Dehydrogenation Catalyzed by Pt Clusters (Pt2–Pt6) in Gas Phase and Supported on g-C3N4 and γ-Al2O3: A Theoretical Study. *ACS Omega* **2025**, *10* (39), 46105-46114. DOI: 10.1021/acsomega.5c07626.

[18] Fricke, C.; Rajbanshi, B.; Walker, E. A.; Terejanu, G.; Heyden, A. Propane Dehydrogenation on Platinum Catalysts: Identifying the Active Sites through Bayesian Analysis. *ACS Catalysis* **2022**, *12* (4), 2487-2498. DOI: 10.1021/acscatal.1c04844.

[19] Zhu, J.; Yang, M.-L.; Yu, Y.; Zhu, Y.-A.; Sui, Z.-J.; Zhou, X.-G.; Holmen, A.; Chen, D. Size-Dependent Reaction Mechanism and Kinetics for Propane Dehydrogenation over Pt Catalysts. *ACS Catalysis* **2015**, *5* (11), 6310-6319. DOI: 10.1021/acscatal.5b01423.

[20] Nykänen, L.; Honkala, K. Density Functional Theory Study on Propane and Propene Adsorption on Pt(111) and PtSn Alloy Surfaces. *The Journal of Physical Chemistry C* **2011**, *115* (19), 9578-9586. DOI: 10.1021/jp1121799.

[21] Wang, J.; Chang, X.; Chen, S.; Sun, G.; Zhou, X.; Vovk, E.; Yang, Y.; Deng, W.; Zhao, Z.-J.; Mu, R.; et al. On the Role of Sn Segregation of Pt-Sn Catalysts for Propane Dehydrogenation. *ACS Catalysis* **2021**, *11* (8), 4401-4410. DOI: 10.1021/acscatal.1c00639.

[22] Yang, M.-L.; Zhu, Y.-A.; Zhou, X.-G.; Sui, Z.-J.; Chen, D. First-Principles Calculations of Propane Dehydrogenation over PtSn Catalysts. *ACS Catalysis* **2012**, *2* (6), 1247-1258. DOI: 10.1021/cs300031d.

[23] Pan, J.; Strugovshchikov, E.; Salóm-Català, A.; Novell-Leruth, G.; Kaźmierczak, K.; Curulla-Ferré, D.; Carbó, J. J.; Godard, C.; Ricart, J. M. Propane Dehydrogenation on Pt Single-Atom and Pt4 and Pt3Sn Single-Cluster Supported on g-C3N4: A Theoretical Study. *The Journal of Physical Chemistry C* **2025**, *129* (5), 2477-2487. DOI: 10.1021/acs.jpcc.4c07686.

[24] Liu, Y.; Zong, X.; Patra, A.; Caratzoulas, S.; Vlachos, D. G. Propane Dehydrogenation on PtxSny (x, y ≤ 4) Clusters on Al2O3(110). *ACS Catalysis* **2023**, *13* (5), 2802-2812. DOI: 10.1021/acscatal.2c05671.

[25] Fricke, C. H.; Bamidele, O. H.; Bello, M.; Chowdhury, J.; Terejanu, G.; Heyden, A. Modeling the Effect of Surface Platinum–Tin Alloys on Propane Dehydrogenation on Platinum–Tin Catalysts. *ACS Catalysis* **2023**, *13* (16), 10627-10640. DOI: 10.1021/acscatal.3c00939.

[26] Liu, D.; Jiang, F.; Zhang, Q.; Huang, W.-H.; Zheng, Y.; Chen, M.; Wu, L.; Qin, R.; Wang, M.; Zhang, S.; et al. Pt–ZnOx Interfacial Effect on the Performance of Propane Dehydrogenation and Mechanism Study. *ACS Nano* **2024**, *18* (51), 34671-34682. DOI: 10.1021/acsnano.4c10030.

[27] Rochlitz, L.; Fischer, J. W. A.; Pessemesse, Q.; Clark, A. H.; Ashuiev, A.; Klose, D.; Payard, P.-A.; Jeschke, G.; Copéret, C. Ti-Doping in Silica-Supported PtZn Propane Dehydrogenation Catalysts: From Improved Stability to the Nature of the Pt–Ti Interaction. *JACS Au* **2023**, *3* (7), 1939-1951. DOI: 10.1021/jacsau.3c00197.

[28] Yang, M.-L.; Fan, C.; Zhu, Y.-A.; Sui, Z.-J.; Zhou, X.-G.; Chen, D. Selective Oxidation of Hydrogen in the Presence of Propylene over Pt-Based Core–Shell Nanocatalysts. *The Journal of Physical Chemistry C* **2015**, *119* (37), 21386-21394. DOI: 10.1021/acs.jpcc.5b03733.

[29] Chang, Q.-Y.; Yin, Q.; Ma, F.; Zhu, Y.-A.; Sui, Z.-J.; Zhou, X.-G.; Chen, D.; Yuan, W.-K. Tuning Adsorption and Catalytic Properties of α-Cr2O3 and ZnO in Propane Dehydrogenation by Creating Oxygen Vacancy and Doping Single Pt Atom: A Comparative First-Principles Study. *Industrial & Engineering Chemistry Research* **2019**, *58* (24), 10199-10209. DOI: 10.1021/acs.iecr.9b01143.

[30] Conley, M. P.; Delley, M. F.; Núñez-Zarur, F.; Comas-Vives, A.; Copéret, C. Heterolytic Activation of C–H Bonds on CrIII–O Surface Sites Is a Key Step in Catalytic Polymerization of Ethylene and Dehydrogenation of Propane. *Inorganic Chemistry* **2015**, *54* (11), 5065-5078. DOI: 10.1021/ic502696n.

[31] Huš, M.; Kopač, D.; Bajec, D.; Likozar, B. Effect of Surface Oxidation on Oxidative Propane Dehydrogenation over Chromia: An Ab Initio Multiscale Kinetic Study. *ACS Catalysis* **2021**, *11* (17), 11233-11247. DOI: 10.1021/acscatal.1c01814.

[32] Jin, D.; Xu, H.; Zhu, J.; Cheng, D. Activation of Cr2O3 for propane dehydrogenation by doping with Pt single-atom promotor. *Molecular Catalysis* **2023**, *551*. DOI: 10.1016/j.mcat.2023.113624.

[33] Li, R.; Zhang, C.; Li, S.; Du, Y. Experimental and theoretical investigations into propane dehydrogenation over MIL-101(Cr/Al) derived catalysts. *Molecular Catalysis* **2023**, *535*. DOI: 10.1016/j.mcat.2022.112894.

[34] Han, S.; Zhao, Y.; Otroshchenko, T.; Zhang, Y.; Zhao, D.; Lund, H.; Vuong, T. H.; Rabeah, J.; Bentrup, U.; Kondratenko, V. A.; et al. Unraveling the Origins of the Synergy Effect between ZrO2 and CrOx in Supported CrZrOx for Propene Formation in Nonoxidative Propane Dehydrogenation. *ACS Catalysis* **2019**, *10* (2), 1575-1590. DOI: 10.1021/acscatal.9b05063.

[35] Dai, G.-L.; Li, Z.-H.; Lu, J.; Wang, W.-N.; Fan, K.-N. Deep Oxidations in the Oxidative Dehydrogenation Reaction of Propane over V2O5(001): Periodic Density Functional Theory Study. *The Journal of Physical Chemistry C* **2011**, *116* (1), 807-817. DOI: 10.1021/jp208639t.

[36] Huang, C.; Wang, Z.-Q.; Gong, X.-Q. Activity and selectivity of propane oxidative dehydrogenation over VO 3 /CeO 2 (111) catalysts: A density functional theory study. *Chinese Journal of Catalysis* **2018**, *39* (9), 1520-1526. DOI: 10.1016/s1872-2067(18)63072-4.

[37] Mokhtari, Z.; Towfighi Darian, J.; Safari Yazd, M. Mechanistic elucidation of MgO-doped VOx@ZrO2 catalysts for enhanced CO2-assisted oxidative dehydrogenation of propane: Tuning oxygen vacancies, spillover, and redox–base properties. *International Journal of Hydrogen Energy* **2025**, *183*. DOI: 10.1016/j.ijhydene.2025.151854.

[38] Liu, Y.; Zhang, T.; Yang, J.; Dong, J.; Fu, Z.; Chu, C.; He, Y.; Bing, L.; Lan, X.; Li, J.; et al. Design and experimental synthesis of VOx/SSZ-13 catalyst based on first principles calculations - elucidating the role of VOx microstructure and valence state in propane dehydrogenation. *Journal of Environmental Chemical Engineering* **2026**, *14* (1). DOI: 10.1016/j.jece.2025.120954.

[39] Shan, Y.-L.; Sun, H.-L.; Zhao, S.-L.; Tang, P.-L.; Zhao, W.-T.; Ding, J.-W.; Yu, W.-L.; Li, L.-N.; Feng, X.; Chen, D. Effects of Support and CO2 on the Performances of Vanadium Oxide-Based Catalysts in Propane Dehydrogenation. *ACS Catalysis* **2022**, *12* (10), 5736-5749. DOI: 10.1021/acscatal.2c00878.

[40] Arinaga, A. M.; Biswas, A.; Zhang, X.; Greeley, J.; Marks, T. J. Origin of Rate and Selectivity Trends and Exceptional Yield in Sulfur-Oxidative Propane Dehydrogenation Over Supported Vanadium Catalysts. *ACS Catalysis* **2023**, *13* (20), 13395-13413. DOI: 10.1021/acscatal.3c03677.

[41] Chen, H.; Gao, P.; Liu, Z.; Liang, L.; Han, Q.; Wang, Z.; Chen, K.; Zhao, Z.; Guo, M.; Liu, X.; et al. Direct Detection of Reactive Gallium-Hydride Species on the Ga2O3 Surface via Solid-State NMR Spectroscopy. *Journal of the American Chemical Society* **2022**, *144* (38), 17365-17375. DOI: 10.1021/jacs.2c01005.

[42] Yuan, Y.; Lee, J. S.; Lobo, R. F. Ga+-Chabazite Zeolite: A Highly Selective Catalyst for Nonoxidative Propane Dehydrogenation. *Journal of the American Chemical Society* **2022**, *144* (33), 15079-15092. DOI: 10.1021/jacs.2c03941.

[43] Bauer, T.; Maisel, S.; Blaumeiser, D.; Vecchietti, J.; Taccardi, N.; Wasserscheid, P.; Bonivardi, A.; Görling, A.; Libuda, J. Operando DRIFTS and DFT Study of Propane Dehydrogenation over Solid- and Liquid-Supported GaxPty Catalysts. *ACS Catalysis* **2019**, *9* (4), 2842-2853. DOI: 10.1021/acscatal.8b04578.

[44] Madubuko, N.; Hsieh, T.-E.; Vorlaufer, N.; Carl, S.; Steffen, J.; Mölkner, A.; Taccardi, N.; Frisch, J.; Wilks, R. G.; Will, J.; et al. Reductive Treatment of Ga–Pt-Supported Catalytically Active Liquid Metal Solutions (SCALMS) for Propane Dehydrogenation. *ACS Catalysis* **2025**, *15* (14), 12436-12449. DOI: 10.1021/acscatal.5c01463.

[45] Raman, N.; Maisel, S.; Grabau, M.; Taccardi, N.; Debuschewitz, J.; Wolf, M.; Wittkämper, H.; Bauer, T.; Wu, M.; Haumann, M.; et al. Highly Effective Propane Dehydrogenation Using Ga–Rh Supported Catalytically Active Liquid Metal Solutions. *ACS Catalysis* **2019**, *9* (10), 9499-9507. DOI: 10.1021/acscatal.9b02459.

[46] Ji, J.; Fan, G.; Zheng, L.; Li, F. Confinement of Atomically Dispersed Ptδ+ Sites in Zinc-Incorporated Silicalite-1 Zeolite for Enhanced Propane Dehydrogenation. *ACS Catalysis* **2025**, *15* (7), 5858-5875. DOI: 10.1021/acscatal.4c07883.

[47] Liu, H.; Chu, B.; Chen, T.; Zhou, J.; Dong, L.; Lo, T. W. B.; Li, B.; He, X.; Ji, H. Modulation of the cobalt species state on zincosilicate to maximize propane dehydrogenation to propylene. *Chinese Journal of Catalysis* **2024**, *66*, 168-180. DOI: 10.1016/s1872-2067(24)60133-6.

[48] Qu, Y.; Li, G.; Zhao, T.; Zhang, Z.; Douthwaite, M.; Zhang, J.; Hao, Z. Low-Temperature Direct Dehydrogenation of Propane over Binary Oxide Catalysts: Insights into Geometric Effects and Active Sites. *ACS Sustainable Chemistry & Engineering* **2021**, *9* (38), 12755-12765. DOI: 10.1021/acssuschemeng.1c03074.

[49] Chen, S.; Chai, Y.; Chen, Y.; Wei, F.; Pan, X.; Lin, J.; Lin, S. Peripheral P doping in Zn1/NC single-atom catalyst to enhance propane dehydrogenation reaction. *Chemical Engineering Science* **2024**, *291*. DOI: 10.1016/j.ces.2024.119919.

[50] Liu, Y.; Liu, Z.; Lu, W.-D.; Wang, D.; Lu, A.-H. In Situ Generated Boron Peroxo as Mild Oxidant in Propane Oxidative Dehydrogenation Revealed by Density Functional Theory Study. *The Journal of Physical Chemistry Letters* **2022**, *13* (50), 11729-11735. DOI: 10.1021/acs.jpclett.2c03341.

[51] Zhuang, J.; Qin, T.; Qi, W.; Cao, L.; Yao, Z.; Hu, M.; Bing, L.; Wang, Y.; Deng, K.; Liu, X. Accelerated Crystallization of Zeolites via Solid Boron Free Radicals. *JACS Au* **2025**, *5* (7), 3374-3386. DOI: 10.1021/jacsau.5c00468.

[52] Wang, G.; Hu, A.; Duan, Q.; Cui, L.; Chen, Z.; Huang, Z.; Zhang, X.; Huang, S.; Xie, Z. Hierarchical boroncarbonitride nanosheets as metal-free catalysts for enhanced oxidative dehydrogenation of propane. *Chemical Engineering Science* **2024**, *288*. DOI: 10.1016/j.ces.2024.119848.

[53] Gao, X.; Cai, C.; Tian, S.; Xu, S.; Lin, L.; Shi, J.; Song, C.; Wang, T.; Ma, D.; Yao, S. Performance Descriptor of Subsurface Metal-Promoted Boron Catalysts for Low-Temperature Propane Oxidative Dehydrogenation to Propylene. *Journal of the American Chemical Society* **2024**, *146* (51), 35165-35174. DOI: 10.1021/jacs.4c11506.

[54] Zhang, X.; Ren, B.; Yang, Z.; Chen, H.; Dai, S. Transforming Boron Carbon Nitride: A Carbon-to-Oxygen Switch to Boost Propane Oxidative Dehydrogenation. *ACS Catalysis* **2025**, *15* (11), 9290-9300. DOI: 10.1021/acscatal.5c01353.

[55] Zhou, Q.; Liu, Z.; Zhu, L.; Lu, W.; He, L.; Wang, D. Oxidative Dehydrogenation of Propane on Boron Phosphate: A Computational Mechanistic Study. *The Journal of Physical Chemistry C* **2023**, *127* (27), 12942-12952. DOI: 10.1021/acs.jpcc.3c00838.

[56] Zhu, L.; Liu, Z.; Zhou, Q.; Lu, W.-D.; Wang, D. Propane Oxidative Dehydrogenation on Nanosized Boron Carbide: Effect of Boron Content and Its Oxidation Implicated by DFT Calculations. *The Journal of Physical Chemistry C* **2023**, *127* (13), 6280-6293. DOI: 10.1021/acs.jpcc.2c08586.

[57] Liu, Y.; Liu, Z.; Wang, D.; Lu, A.-H. Suppressing Deep Oxidation by Detached Nano-sized Boron Oxide in Oxidative Dehydrogenation of Propane Revealed by the Density Functional Theory Study. *The Journal of Physical Chemistry C* **2022**, *126* (50), 21263-21271. DOI: 10.1021/acs.jpcc.2c06910.

[58] Chang, X.; Lu, Z.; Luo, R.; Wang, X.; Sun, G.; Fu, D.; Zhao, Z.-J.; Gong, J. Microenvironment engineering of non-noble metal alloy for selective propane dehydrogenation. *Chem* **2025**, *11* (1). DOI: 10.1016/j.chempr.2024.08.017.

[59] Liang, K.; Zeng, X.; Dang, L.; Li, S. Structure Sensitivity Study of Propane Dehydrogenation on Cobalt Catalysts: HCP versus FCC. *The Journal of Physical Chemistry C* **2023**, *127* (37), 18409-18419. DOI: 10.1021/acs.jpcc.3c05358.

[60] Li, C.-F.; Guo, X.; Shang, Q.-H.; Yan, X.; Ren, C.; Lang, W.-Z.; Guo, Y.-J. Defective TiO2 for Propane Dehydrogenation. *Industrial & Engineering Chemistry Research* **2020**, *59* (10), 4377-4387. DOI: 10.1021/acs.iecr.9b06759.

[61] Zhang, Y.; Zhao, Y.; Otroshchenko, T.; Perechodjuk, A.; Kondratenko, V. A.; Bartling, S.; Rodemerck, U.; Linke, D.; Jiao, H.; Jiang, G.; et al. Structure–Activity–Selectivity Relationships in Propane Dehydrogenation over Rh/ZrO2 Catalysts. *ACS Catalysis* **2020**, *10* (11), 6377-6388. DOI: 10.1021/acscatal.0c01455.

[62] Araujo-Lopez, E.; Joos, L.; Vandegehuchte, B. D.; Sharapa, D. I.; Studt, F. Theoretical Investigations of (Oxidative) Dehydrogenation of Propane to Propylene over Palladium Surfaces. *The Journal of Physical Chemistry C* **2020**, *124* (5), 3171-3176. DOI: 10.1021/acs.jpcc.9b11424.

[63] Saelee, T.; Namuangruk, S.; Kungwan, N.; Junkaew, A. Theoretical Insight into Catalytic Propane Dehydrogenation on Ni(111). *The Journal of Physical Chemistry C* **2018**, *122* (26), 14678-14690. DOI: 10.1021/acs.jpcc.8b03939.

[64] Li, Y.; Yang, X. Unveiling the Catalytic Mechanism and Selectivity Control Strategies of Two-Dimensional C3N Materials for Propane Oxidative Dehydrogenation: A DFT Study. *The Journal of Physical Chemistry C* **2025**, *129* (43), 19336-19346. DOI: 10.1021/acs.jpcc.5c03202.

[65] Yu, J.; Xu, Y.; Guliants, V. V. Propane ammoxidation over Mo–V–Te–Nb–O M1 phase: Density functional theory study of propane oxidative dehydrogenation steps. *Catalysis Today* **2014**, *238*, 28-34. DOI: 10.1016/j.cattod.2014.02.053.

[66] Dou, J.; Funderburg, J.; Yang, K.; Liu, J.; Chacko, D.; Zhang, K.; Harvey, A. P.; Haribal, V. P.; Zhou, S. J.; Li, F. CexZr1–xO2-Supported CrOx Catalysts for CO2-Assisted Oxidative Dehydrogenation of Propane─Probing the Active Sites and Strategies for Enhanced Stability. *ACS Catalysis* **2022**, *13* (1), 213-223. DOI: 10.1021/acscatal.2c05286.

[67] Zhai, P.; Xie, Z.; Huang, E.; Aireddy, D. R.; Yu, H.; Cullen, D. A.; Liu, P.; Chen, J. G.; Ding, K. CO2-mediated oxidative dehydrogenation of propane enabled by Pt-based bimetallic catalysts. *Chem* **2023**, *9* (11), 3268-3285. DOI: 10.1016/j.chempr.2023.07.002.

[68] Nie, X.; Zhao, S.; Liu, T.; Qu, S.; Fan, H.; Song, C.; Guo, X. Computational Identification of Catalytic Mechanism and Performance of Pt4/Fe-MFI Catalyst for Propane Dehydrogenation. *Energy & Fuels* **2025**, *39* (37), 18053-18065. DOI: 10.1021/acs.energyfuels.5c02867.

[69] Yang, Y.; Liao, R.; Pu, R.; Jiang, P.; Li, L.; Wang, X.; Ji, H. A new isopropanol-intermediate mechanism for CO2-assisted propane dehydrogenation over ZIF-derived (GaCe)Ox: Toward propylene synthesis. *Chemical Engineering Journal* **2025**, *525*. DOI: 10.1016/j.cej.2025.170285.

[70] Seemakurthi, R. R.; Canning, G.; Wu, Z.; Miller, J. T.; Datye, A. K.; Greeley, J. Identification of a Selectivity Descriptor for Propane Dehydrogenation through Density Functional and Microkinetic Analysis on Pure Pd and Pd Alloys. *ACS Catalysis* **2021**, *11* (15), 9588-9604. DOI: 10.1021/acscatal.1c01916.

[71] Yang, T.; Zhong, Y.; Li, J.; Ma, R.; Yan, H.; Liu, Y.; He, Y.; Li, D. Construction of a Unique Structure of Ru Sites in the RuP Structure for Propane Dehydrogenation. *ACS Applied Materials & Interfaces* **2021**, *13* (28), 33045-33055. DOI: 10.1021/acsami.1c07842.

[72] Bunting, R. J.; Wodaczek, F.; Torabi, T.; Cheng, B. Reactivity of Single-Atom Alloy Nanoparticles: Modeling the Dehydrogenation of Propane. *Journal of the American Chemical Society* **2023**, *145* (27), 14894-14902. DOI: 10.1021/jacs.3c04030.

[73] Wang, X.; Zhao, H.; Ma, Y.; Wang, L.; Li, Y.; Chi, L. Discovery of promising Cu-based catalysts for selective propane dehydrogenation to propylene assisted by high-throughput computations. *Journal of Catalysis* **2024**, *438*. DOI: 10.1016/j.jcat.2024.115718.

[74] Wang, X.; Zhao, H.; Ma, Y.; Wang, L.; Li, Y.; Chi, L. Discovery of promising Cu-based catalysts for selective propane dehydrogenation to propylene assisted by high-throughput computations. *Journal of Catalysis* **2024**, *438*. DOI: 10.1016/j.jcat.2024.115718.

[75] Sun, X.; Han, P.; Li, B.; Zhao, Z. Tunable Catalytic Performance of Single Pt Atom on Doped Graphene in Direct Dehydrogenation of Propane by Rational Doping: A Density Functional Theory Study. *The Journal of Physical Chemistry C* **2018**, *122* (3), 1570-1576. DOI: 10.1021/acs.jpcc.7b09736.

[76] Montemore, M. M.; Medlin, J. W. Site-Specific Scaling Relations for Hydrocarbon Adsorption on Hexagonal Transition Metal Surfaces. *The Journal of Physical Chemistry C* **2013**, *117* (39), 20078-20088. DOI: 10.1021/jp4076405.

[77] Kong, N.; Fan, X.; Liu, F.; Wang, L.; Lin, H.; Li, Y.; Lee, S.-T. Single Vanadium Atoms Anchored on Graphitic Carbon Nitride as a High-Performance Catalyst for Non-oxidative Propane Dehydrogenation. *ACS Nano* **2020**, *14* (5), 5772-5779. DOI: 10.1021/acsnano.0c00659.

[78] Hou, W.; Lin, K.; Zhang, X.; Xu, B.; Wang, Y.; Lu, X.; Gao, Y.; Ma, R.; Fu, Y.; Zhu, W. Highly stable and selective Pt/TS-1 catalysts for the efficient nonoxidative dehydrogenation of propane. *Chemical Engineering Journal* **2023**, *474*. DOI: 10.1016/j.cej.2023.145648.

[79] Chen, T.; Zhao, S.; Lin, J.; Chong, Y.; Li, Y.; Zhao, Y.; Chen, G.; Qiu, Y. Theoretical and experimental study on the dehydrogenation of propane by oxygen vacancy caused by γ-Al2O3 with the assistance of S. *Surfaces and Interfaces* **2023**, *42*. DOI: 10.1016/j.surfin.2023.103399.

[80] Wu, R.; Chen, B.; Liu, N.; Dai, C.; Xu, R.; Yu, G.; Wang, N.; Xu, Y.; Han, H. NiCrOx@silicalite-1 with Advanced CO2Utilization in Oxidative Dehydrogenation of Propane: Insights into Bifunctional Catalysis and Reaction Efficiency. *ACS Sustainable Chemistry & Engineering* **2025**, *13* (23), 8644-8659. DOI: 10.1021/acssuschemeng.5c02033.